Analysis of Mesovortex Characteristics, Behavior, and Interactions during the Second 30 June–1 July 2014 Midwestern Derecho Event

ANTHONY W. LYZA, ADAM W. CLAYTON, AND KEVIN R. KNUPP
Department of Atmospheric Science, Severe Weather Institute—Radar and Lightning Laboratories
University of Alabama in Huntsville, Huntsville, Alabama

ERIC LENNING, MATTHEW T. FRIEDLEIN, AND RICHARD CASTRO
NOAA/National Weather Service, Romeoville, Illinois

EVAN S. BENTLEY
NOAA/National Weather Service, Portland, Oregon

(Submitted 19 February 2017; in final form 25 August 2017)

ABSTRACT

A pair of intense, derecho-producing quasi-linear convective systems (QLCSs) impacted northern Illinois and northern Indiana during the evening hours of 30 June through the predawn hours of 1 July 2014. The second QLCS trailed the first one by only 250 km and approximately 3 h, yet produced 29 confirmed tornadoes and numerous areas of nontornadic wind damage estimated to be caused by 30–40 m s^{-1} flow. Much of the damage from the second QLCS was associated with a series of 38 mesovortices, with up to 15 mesovortices ongoing simultaneously. Many complex behaviors were documented in the mesovortices, including: a binary (Fujiwhara) interaction, the splitting of a large mesovortex in two followed by prolific tornado production, cyclic mesovortexgenesis in the remains of a large mesovortex, and a satellite interaction of three small mesovortices around a larger parent mesovortex. A detailed radar analysis indicates no definitive differences between tornadic and nontornadic mesovortices. All observed mesovortices were cyclonic, indicating that either the vertical tilting of streamwise vorticity, generation of vortices via the release of horizontal shearing instability, or both were involved in mesovortex genesis. This paper examines the environment ahead of the second QLCS, the characteristics of the mesovortices produced, and the aforementioned complex interactions. It also discusses implications for mesovortex genesis and dynamics as well as operational considerations.

———————————————

1. Introduction

Organized mesoscale convective systems (MCSs) often evolve into quasi-linear convective systems (QLCSs) that can produce a range of severe convective hazards. The most notable hazards are flash floods, damaging nontornadic thunderstorm winds, and tornadoes of typically

Corresponding author address: Anthony W. Lyza, Department of Atmospheric Science, University of Alabama in Huntsville, 4801 Bradford Dr., Huntsville, AL, 35805
Email: lyzaa@nsstc.uah.edu

EF2 or lesser rating on the Enhanced Fujita scale (WSEC 2006; Trapp et al. 2005; Smith et al. 2012). Bow echoes (e.g. Weisman 1993), associated with the descent of a rear-inflow jet (RIJ) to the surface (e.g. Smull and Houze 1987; Weisman 1992, 1993), have been identified as a primary cause of nontornadic damaging winds with QLCSs. Tornadoes are most likely to occur immediately to the north of the apex of a bowing segment or within the comma-head region at the northern end of the bow echo (Fujita 1978, 1981; Wakimoto 1983; Przybylinski 1995; Pfost and Gerard 1997; Funk et al. 1999; Weisman and Trapp 2003; Atkins et al. 2004, Atkins et al. 2005).

QLCS tornadoes have been well-documented in the literature, including events with numerous tornadoes (Forbes and Wakimoto 1983; Knupp et al. 2014; Skow and Cogil 2017). A climatology by Trapp et al. (2005) found that ≈18% of tornadoes are produced by QLCSs. Though they tend to be weaker than their supercellular counterparts, ≈11% were documented by Smith et al. (2012) to have reached F2/EF2 levels, the highest-rated being F4 (Wakimoto 1983). Observational and numerical-simulation results suggest that mesovortices also are associated with the strongest nontornadic winds in a QLCS (Wakimoto et al. 2006a). These maximum winds are most likely where a mesovortex is superimposed with a descending RIJ (Atkins and St. Laurent 2009a; Wakimoto et al. 2006b).

The Midwestern United States is a climatologically favored area for QLCS tornadoes, particularly during the summer months (Smith et al. 2012). Climatologies of progressive derecho paths show a peak corridor across the upper Midwest to the southern Great Lakes, particularly from central and southern Minnesota to western and central Ohio (Johns and Hirt 1987; Coniglio and Stensrud 2004). Guastini and Bosart (2016) specifically found a maximum that included northern Illinois and northern Indiana.

Given the QLCS climatology, it was not unusual to see a pair of tornadic QLCSs impact the upper Mississippi River Valley and southern Great Lakes region between the midday hours of 30 June and the early overnight hours of 1 July 2014. More surprising was the evolution of these two events in close succession. The first QLCS grew upscale from a cluster of supercells that produced 11 tornadoes across central and eastern Iowa, before slowly dissipating over Lower Michigan. The second QLCS developed across central and eastern Iowa only 250 km behind, and less than three hours after, the first QLCS. It then strengthened across northern Illinois, producing 29 confirmed tornadoes from a series of 38 identified mesovortices over a period of ≈4 h. As many as 15 mesovortices were occurring simultaneously. In most cases, these mesovortices were located on or near the leading edge of convection.

Tornadoes associated with leading-edge mesovortices, as during the 30 June 2014 event, pose a particular challenge to National Weather Service (NWS) warning operations. Brotzge et al. (2013) indicated a probability of detection (POD) as low as 48% for QLCS tornadoes during their study period. Trapp et al. (1999) found that tornado vortex signatures (TVSs) associated with QLCSs tended to be non-descending in their evolution and linked to less tornado-warning lead time. Less skill has been displayed in warning for QLCS tornadoes than for discrete supercell tornadoes, with a higher percentage of unwarned QLCS tornadoes than of unwarned supercell tornadoes (Brotzge and Erickson 2010). The difficulties associated with warning for QLCS tornadoes lessen lead time for tornado warnings as a whole in the midwestern and southeastern United States, versus the Great Plains (Brotzge and Erickson 2009).

A key reason for these operational challenges is that the genesis and evolution of leading-edge mesovortices, the parent circulations of tornadoes associated with QLCSs, are not fully understood. Several hypotheses have been developed through idealized or semi-idealized numerical simulations (Trapp and Weisman 2003; Wheatley and Trapp 2008; Atkins and St. Laurent 2009b; Schenkman and Xue 2016). Multiple research efforts (Atkins et al. 2004, Schaumann and Przybylinski 2012, Stanford et al. 2014) also have sought to aid operational warning forecasters by developing techniques for assessing the tornadic potential of mesovortices in a QLCS, with varying degrees of success (NWS Springfield 2016).

Recently deployed radar technologies such as dual-polarization and the Supplemental Adaptive Intra-Volume Low-Level Scan technique (SAILS; ROC 2012) aid the detection and tracking of storm-scale features such as mesovortices and tornadic debris signatures (TDS; e.g. Ryzhkov et al. 2005; Schultz et al. 2012). The present study uses these recent as well as more established radar technologies to analyze of mesovortex behavior during the second QLCS of 30 June–1 July 2014. Beyond documenting unique interactions and behaviors of these mesovortices, this study offers more insight on the most likely mechanisms governing mesovortex generation and evolution. The goal is to help improve warning lead time and accuracy for similar events in the future.

2. Summary of the QLCS development and environment

Iowa and northern Illinois experienced multiple rounds of severe convection in late June 2014. On the morning of 30 June, the latest cluster of storms initiated in eastern Nebraska and quickly grew upscale as it began to forward propagate through Iowa. By the afternoon this cluster had moved into southern Wisconsin and evolved into a severe bowing MCS with over 100 reports of wind damage or severe wind speeds along its path (NCEI 2016). Additional storms developing on the southern flank of the bow across northern Illinois quickly organized into a line. This line pushed into Lower Michigan and northern Indiana around 0100 UTC but weakened as it outran the deep layer shear and greater instability.

As the lead convective line was moving across Illinois and Wisconsin between 2100 and 0000 UTC, new convection was forming in central and eastern Iowa. This line quickly organized into a QLCS across northwestern and north-central Illinois (Fig. 1) and several mesovortices began to form as the QLCS encountered the cold pool from the first convective system. At least 10 these mesovortices eventually became tornadic, with 29 confirmed tornadoes from this second QLCS across Illinois and Indiana (Fig. 2). The QLCS continued into northeastern Indiana during the overnight hours. Its gust front outran the convective line, as indicated by radar and observations, and gradually decayed between 0500–0800 UTC 1 July.

The magnitude and longevity of these two convective lines met both the traditional and the recently proposed revision to the definition of a derecho (Johns and Hirt 1987, Corfidi et al. 2016). Both systems generated a swath of wind damage reports around 700 km long and 200 km wide. The area of maximum intensity for both systems was around 400 km long, during which they produced numerous tornadoes, measured gusts >64 kt (33 m s^{-1}), or damage indicating winds of that magnitude.

Support for these derechos was provided in part by a seasonally strong 500-hPa jet stream wrapping around a deepening upper low across central Canada, together with warm and moist return flow at low levels. On the afternoon of 30 June, a shortwave trough associated with the upper low was positioned over the northern Plains. By 0000 UTC 1 July, this trough had

Figure 1: Radar base reflectivity mosaic across the midwestern United States at 2230 UTC 30 June 2014 (top), 0130 UTC 1 July 2014 (middle), and 0430 UTC 1 July 2014 (bottom), showing the evolution of the two derecho-producing QLCSs. Mosaic images from Iowa Environmental Mesonet NEXRAD composite archive. *Click image to enlarge.*

moved into the northern Great Lakes and deepened with concurrent strengthening of the upper-level jet near Lake Superior. A cold frontextended from an occluding 984-hPa low in Ontario through central Wisconsin and into southern Iowa and northern Missouri, where a weaker secondary 1002-hPa low was present (Fig. 3).
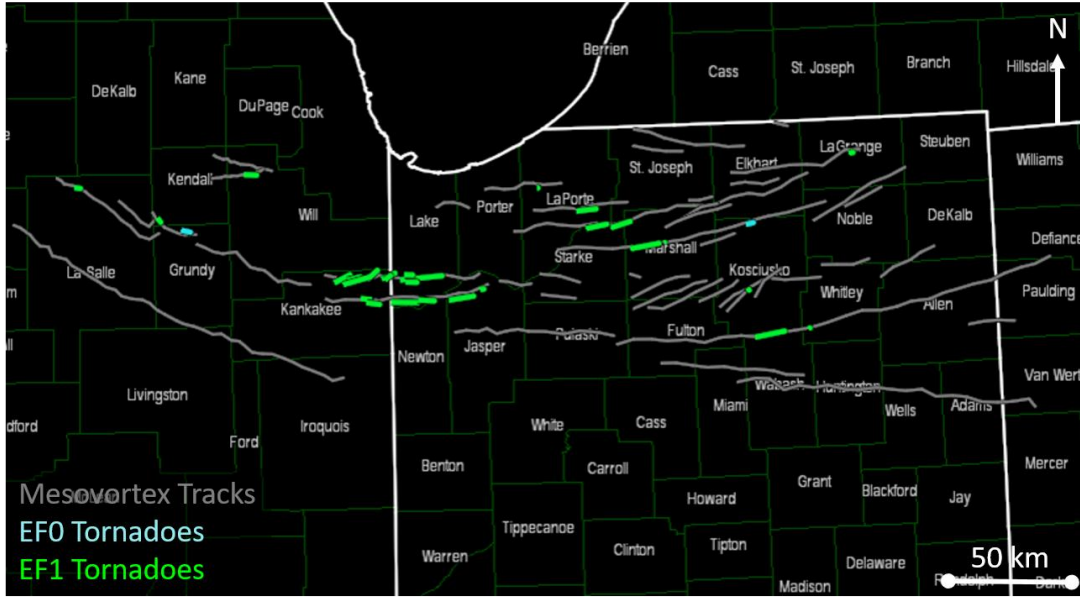
Figure 2: Track map of all mesovortices (gray) and confirmed tornadoes (colored as in legend) during the second 30 June–1 July 2014 derecho. *Click image to enlarge and to view labels for mesovortices described in the text.*
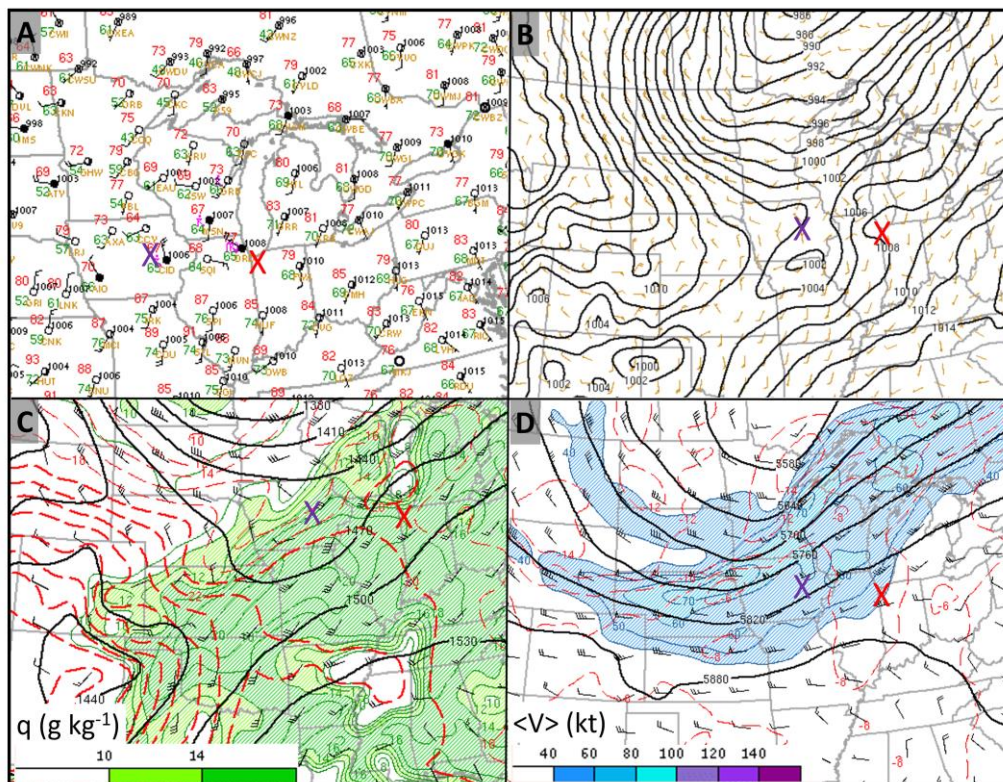

Figure 3: 0000 UTC 1 July 2014: a) surface observations; b) sea-level pressure (hPa); c) 850-hPa temperature (red dashed), heights (black solid), wind (barbs) and mixing ratio (q; green shaded); and d) 500-hPa temperature (red dashed), height (black solid), isotachs (blue shaded), and wind (barbs). Red and purple "X" symbols denote centroids of the first and second QLCSs, respectively. Maps from the Storm Prediction Center's mesoanalysis archive. *Click image to enlarge.*
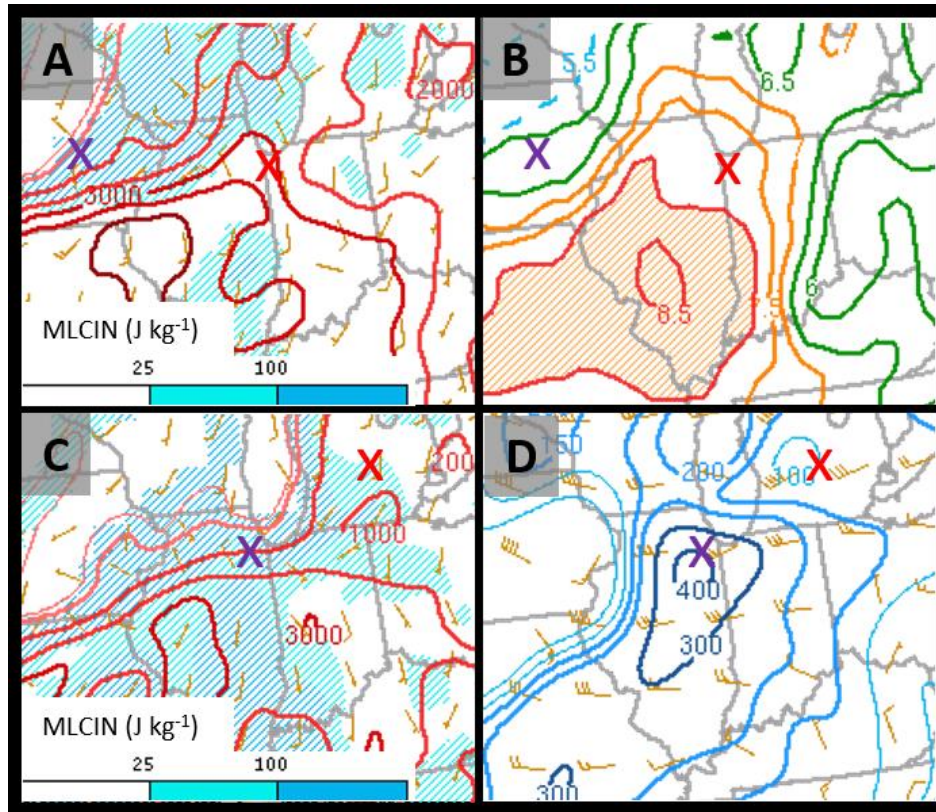
<u>Figure 4</u>: a) 0000 UTC 1 July 2014 MLCAPE (red solid contours, J kg^{-1}), ML convective inhibition (MLCIN; blue shading, J kg^{-1}) and surface wind (barbs); b) 0000 UTC 700–500-hPa temperature lapse rates (°C km^{-1}); c) as in part (a) but at 0300 UTC 1 July 2014; and d) 0300 UTC 1 July 2014 0–1-km storm-relative helicity (SRH; blue solid contours, m^2 s^{-2}) and storm motion vectors (barbs). Red and purple "X" markers as in Fig. 3. Maps from the Storm Prediction Center's mesoanalysis archive. *Click image to enlarge.*

Mesoanalysis data from the Storm Prediction Center (SPC 2016) indicated a strongly unstable environment ahead of both lines as well as the veering of low-level winds with height, also supporting severe convection. Ahead of the cold front, southerly surface winds had advected 23–25°C dewpoints into north central Illinois and Indiana by 0000 UTC 1 July. Above this humid boundary layer, the eastward progression of a Plains elevated mixed layer [EML (Lanicci and Warner 1991); Fig. 3] produced steep mid-level lapse rates (7.5 to 8.5 °C km^{-1}; Fig. 4). This EML together with the warm and humid boundary layer generated mixed-layer (ML) CAPE values of 3000–4000 J kg^{-1}. Furthermore, winds increased to 18 to 21 m s^{-1} (35–40 kt) out of the southwest at 850 hPa with a developing low-level jet, and to 26–31 m s^{-1} (50–60 kt) out of the west at 500 hPa (Fig. 3).

After 0000 UTC, as the first QLCS moved through, the larger MLCAPE shifted southward

but remained >2000 J kg^{-1} across north-central Indiana ahead of the second convective complex. The 850-hPa low-level jet continued to strengthen into the late evening hours and reached 23–26 m s^{-1} (45–50 kt) by 0300 UTC 1 July. This, along with backing of the surface flow in the wake of the first QLCS, led to 0–1-km storm-relative helicity (SRH) of 300–400 m^2 s^{-2} per SPC mesoanalysis (Fig. 4). Aircraft soundings and velocity azimuth display wind profiles indicated even higher values (Fig. 5).

Friedlein et al. (2015) describe in greater detail how this combination of strong low-level wind shear, ambient environmental vorticity left by the cold pool from the first QLCS, and a moderately unstable environment provided the catalyst for the prolific tornadic environment during the evening of 30 June. Most importantly, a surface boundary associated with the southern extent of the cold pool from the first
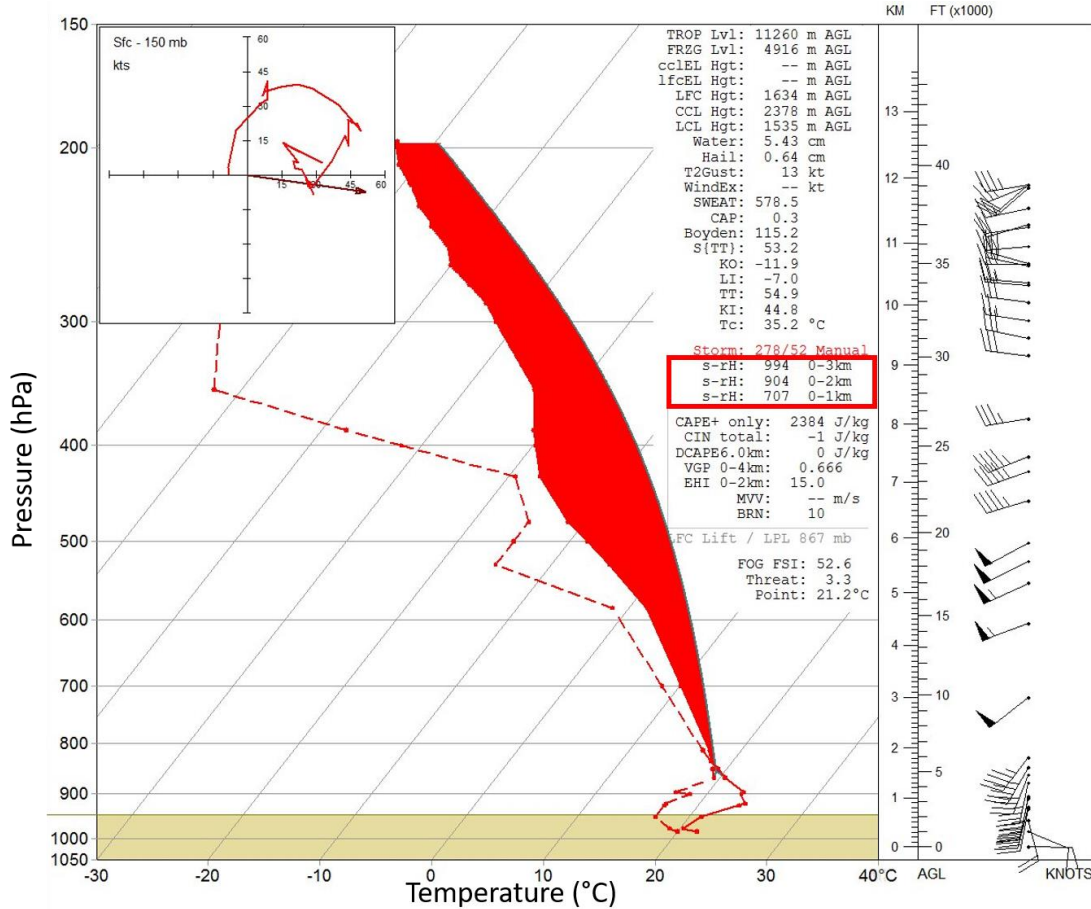
Figure 5: Skew *T*–log*p* plot and inset hodograph from the 0237 UTC KMDW Aircraft Meteorological Data Relay (WMO AMDAR Panel 2007) sounding. The parcel path and shaded region represent an MU parcel and MUCAPE, respectively. *Click image to enlarge.*

QLCS appeared to play a key role in the evolution of the second QLCS and its prolific tornado production. As the first line moved out of the area, its outflow boundary took on the characteristics of a warm front as it moved back north under the influence of warm and moist southerly flow (Fig. 6). The mesovortex and tornado activity with the second QLCS was concentrated along and just north of this advancing boundary for most of its lifecycle. Such interaction between convection and shallow baroclinic zones long has been recognized as favorable for the development of severe tornadic storms (e.g., Maddox et al. 1980; Markowski et al. 1998).

3. Data and methodology

Imagery from WSR-88D units in northern parts of Illinois and Indiana formed the primary dataset for this study: Chicago/Romeoville, IL

(KLOT) and Syracuse, IN (KIWX). Additionally, the terminal Doppler weather radar for Chicago-Midway International Airport (TMDW), located 15 mi (24 km) south-southwest of Chicago, IL, served for the analysis of two mesovortices that passed directly over KLOT. Radar analysis was performed using the Gibson Ridge Level 2 (GRLevel2) Analyst Edition for KLOT and KIWX data, while GibsonRidge Level 3 (GRLevel3) was used to analyze TMDW data.

Each of the 38 mesovortices was assigned an alphanumeric identifier in order of the time each first was detected. For mesovortices that formed at the same radar time, identifiers were assigned from northernmost to southernmost. The first 26 mesovortices were identified by letters "A" through "Z", while the last 12 mesovortices were identified as "AA" through "AL". Peak rotational velocity (V_{ROT}; Brown et al. 1978) was

rounded to 10 m s^{-1} or greater on a 0.5° beam-tilt base velocity scan for all but two features denoted as mesovortices, with the other two vortices over 70 km from the nearest radar site. The following three criteria were used to add confidence to mesovortex identification:

1. A TDS or similar depression in cross-polar correlation coefficient (ρ_{hv}), likely from debris that in most cases met the criteria defined by Clayton et al. (2016) and Skow and Cogil (2017);

2. Confirmation of a tornado through NWS damage surveys; and/or

3. Reports of damage collocated with an area of rotation on radar lasting at least two consecutive 0.5° base velocity scans and exhibiting vertical continuity above 0.5°.

V_{ROT} was calculated using the following equation:

$$V_{ROT} = (V_{max} - V_{min}) \times \cos(\theta) / 2. \quad (1)$$

Here V_{max} and V_{min} are the maximum outbound and inbound radial velocities, respectively, and θ is the angular offset between the radial positions of V_{max} and V_{min}. Note that $\theta = 0$ if V_{max} and V_{min} are located the same distance from the measuring radar (Desrochers and Harris 1996). The use of θ includes only the rotational (tangential) component of flow in the calculation of V_{ROT} and excludes any convergent (radial) component.
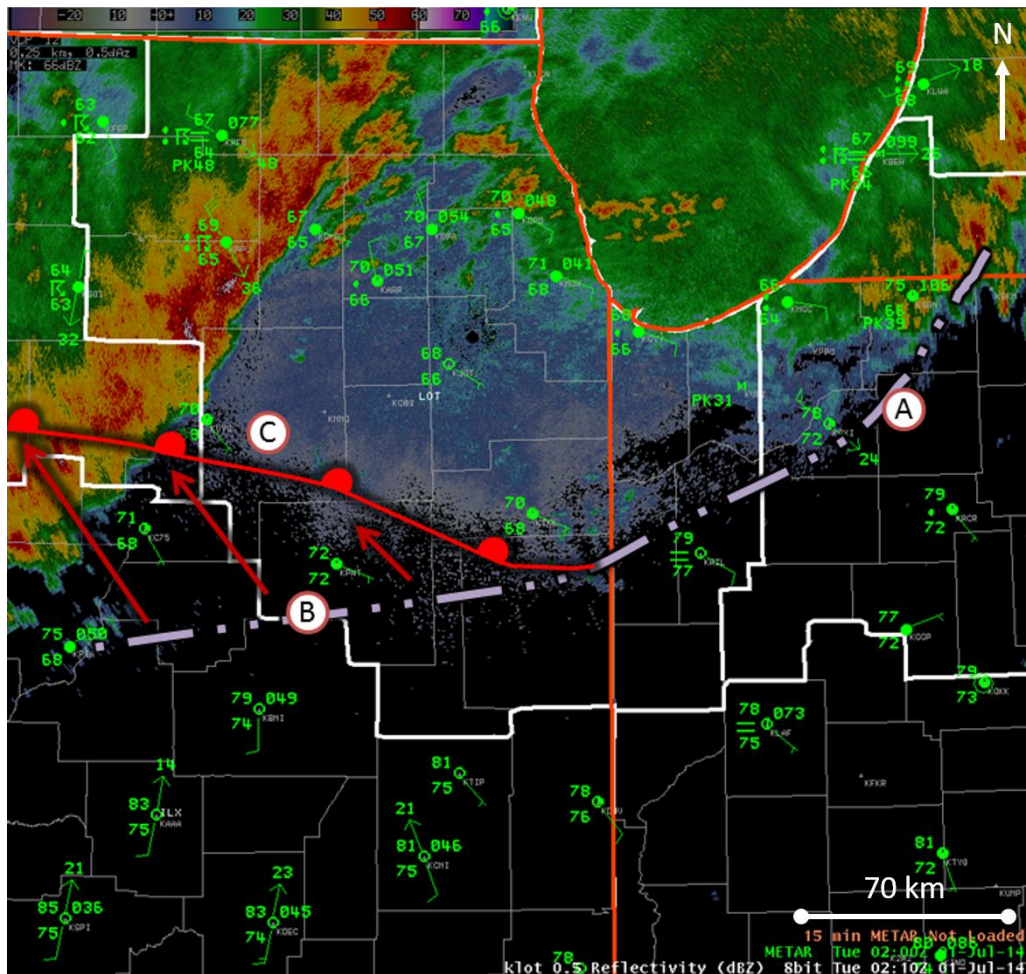
Figure 6: Map of surface station plots (temperature and dewpoints in °F, MSL pressure in hPa, and wind in kt) and radar reflectivity factor (*Z*) from the KLOT WSR-88D radar at 0200 UTC. The following features are indicated: a) the leading edge of the cold pool from the first line at 0200 UTC; b) the southernmost extent of the cold pool from the first line; and c) the 0200 UTC position of the mesoscale warm front as the cold pool moves north. *Click image to enlarge.*

Mesovortex diameters were approximated by the distance between the 0.5° V_{max} and V_{min} at each volume time. To avoid confusion, no distinction was made between vortices that reached meso-γ scale (diameter of 2–20 km; Orlanski 1975) and those that were smaller (often called "misovortices"). Nine of the 38 identified vortices fell short by 2 km in maximum diameter to fit the Orlanski definition of meso-γ scale[1]. Vortices below this threshold have been termed "misovortices" in some literature (Wilczak et al. 1992; Lee and Wilhelmson 1997; Friedrich et al. 2005; Arnott et al. 2006; Murphey et al. 2006; Marquis et al. 2007; Buban et al. 2007; Steiger et al. 2013; Buban and Ziegler 2016). In this paper, the term "mesovortex" is used to describe all vortices that match the previously listed criteria. This was done in order to maintain continuity with past literature on these vortices associated with QLCSs (e.g. Trapp and Weisman 2003; Weisman and Trapp 2003; Atkins et al. 2004; Wakimoto et al. 2006a,b; Wheatley et al. 2006; Wheatley and Trapp 2008; Atkins and St. Laurent 2009a,b; Schaumann and Przybylinski 2012; Stanford et al. 2014; NWS Springfield 2016; Schenkman and Xue 2016). This also avoids the need for two naming conventions based on whether a vortex fits into "meso-" or "miso-" length scales.

- Table 1 summarizes key properties of each of the 38 documented mesovortices. To evaluate their characteristics, mesovortices were first divided into three categories:

- Confirmed-tornadic: those that produced tornadoes confirmed by damage surveys;

- Possibly tornadic: those that may have produced tornadoes but no tornadoes officially were confirmed; and

- Nontornadic: those that did not produce any confirmed tornadoes and for which no tornadoes reasonably are suspected.

Two separate analyses of mesovortex characteristics were performed. The first discretely compared the three categories described above while the second combined possibly tornadic and confirmed-tornadic mesovortices. Once sorted, evaluated characteristics included:

- Maximum V_{ROT};
- Maximum depth;
- Maximum diameter at 0.5° elevation angle;
- Distance traveled;
- Duration; and
- Mean translational speed.

The official *Storm Data* documentation was used to classify the "confirmed-tornadic" mesovortices (NCEI 2016). However, mesovortices that were designated "possibly tornadic" were not documented in Storm Data as tornadic, but showed evidence of likely polarimetric TDSs (e.g. Ryzhkov et al. 2005) and/or had reports of damage collocated with <3-km diameter Doppler velocity couplets.

4. Unique characteristics, behaviors, and observations of selected mesovortices

The extensive number and close proximity of mesovortices led to unique behaviors in several of the mesovortices during the event. The behaviors described represent a highest-confidence description of the evolutions of the mesovortices. Spatial and temporal resolution of the available radar data limit exact behavior identification and introduce analytic uncertainty.

a. Binary interaction between mesovortices "E" and "F"

A pair of mesovortices was identified across northeastern Illinois within 20 km of the Chicago NWS forecast office and KLOT radar site. These mesovortices, named mesovortices "E" and "F" in the standardized nomenclature for this case, were responsible for widespread wind damage and one confirmed tornado in the southwestern suburbs of Chicago. The location of this mesovortex was also within close proximity of TMDW, which was operating in a three-tilt, (0.3°, 0.7°, and 1.3°), one-minute volume coverage pattern. This high-resolution low-level radar data allowed for detailed documentation of the two mesovortices and their interaction with each other.

Both mesovortices "E" and "F" first became apparent on the TMDW radar at 0247 UTC. The initial separation between the two mesovortices' centroids was ≈9.2 km. As shown in Fig. 7, "E" and "F" gradually moved closer together as they intensified, while "F" produced an EF1 tornado

---

[1] Fujita (1981) used an even higher threshold of 4 km for "mesoscale" features.

Table 1: Overview of characteristics of all 38 recorded mesovortices associated with the second QLCS. Red entries indicate mesovortices that produced confirmed tornadoes, blue entries indicate mesovortices with possible tornadoes based on radar data and/or damage reports, and non-highlighted entries indicate an absence of tornadoes.

Mesovortex ID	Start Time (UTC)	End Time (UTC)	Duration (HH:MM:SS)	Distance Traveled (km)*	Max 0.5° V_{ROT} (m s^{-1})	Max 0.5° Diameter (km)	Max Depth (km)**
A	2:05:19	3:38:15	1:32:56	137.20	22.8	7.3	2.7
B	2:10:37	2:39:07	0:38:30	44.14	14.5	4.7	3.9
C	2:26:50	2:39:07	0:12:43	15.78	19.0	2.9	2.4
D	2:36:36	2:48:36	0:12:00	18.71	22.5	6.4	1.1
E	2:47:36	3:04:32	0:16:56	23.11	15.8	5.2	N/A
F	2:47:36	2:59:36	0:12:00	20.02	12.2	2.2	N/A
G (Part 1)	2:48:36	3:16:54	0:28:18	45.78	28.9	13.2	1.8
G-1	3:19:46	3:59:35	0:39:49	58.33	29.2	7.7	8.8
G-2	3:19:46	3:59:35	0:39:49	61.53	28.2	8.8	3.6
G (Part 2)	4:02:27	4:10:15	0:07:48	12.29	22.2	12.1	3.5
G-3	4:14:05	4:22:39	0:08:34	15.23	7.7	4.0	2.9
G-4	4:14:05	4:22:39	0:08:34	13.00	14.2	6.7	2.7
H	3:43:34	3:54:14	0:10:40	12.53	9.9	2.1	2.8
I	3:54:14	4:35:30	0:41:16	59.95	19.2	6.1	4.1
J	3:57:07	4:18:22	0:21:15	28.99	18.2	6.8	5.0
K	4:04:55	5:22:38	1:17:43	112.70	26.5	6.0	5.7
L	4:10:15	4:35:30	0:25:15	35.61	16.6	4.9	4.1
M	4:18:22	5:22:38	1:04:16	102.60	27.0	4.5	N/A
N	4:35:30	5:05:30	0:30:00	42.15	23.5	6.5	5.8
O	4:35:30	4:48:22	0:12:52	18.93	17.8	4.9	3.7
P	4:35:30	4:39:48	0:04:18	4.22	10.8	2.9	5.3
Q	4:35:30	4:52:39	0:17:09	23.29	10.6	4.1	4.1
R	4:35:30	4:56:55	0:21:25	29.70	10.1	3.7	5.3
S	4:35:30	6:27:00	1:52:00	166.70	19.2	7.2	3.3
T	4:39:48	5:01:13	0:21:25	29.95	13.0	3.7	5.4
U	4:44:05	4:56:55	0:12:50	21.80	14.8	2.7	3.4
V	4:48:22	4:56:55	0:08:33	8.98	19.5	3.0	3.7
W	4:48:22	5:01:13	0:12:51	21.63	11.9	2.1	2.7
X	4:48:22	5:26:56	0:38:34	53.90	15.1	2.9	3.0
Y	4:52:39	5:01:13	0:08:34	13.89	9.6	2.1	0.7
Z	4:52:39	5:05:30	0:12:51	16.60	14.7	1.5	5.3
AA	4:56:55	5:05:30	0:08:35	12.88	16.0	1.4	2.0
AB	4:56:55	5:26:56	0:30:01	37.84	24.5	5.8	N/A
AC	5:01:13	5:35:32	0:34:19	49.54	24.0	5.7	3.9
AD	5:01:13	5:14:04	0:12:51	18.32	20.6	4.6	3.8
AE	5:01:13	5:09:47	0:08:35	14.50	14.8	1.9	1.7
AF	5:09:47	5:14:04	0:04:17	5.51	21.8	4.0	3.3
AG	5:09:47	6:35:35	1:25:48	112.80	18.5	7.2	4.5
AH	5:18:21	5:44:06	0:25:45	40.17	13.3	1.9	4.7
AI	5:26:56	5:35:32	0:08:36	15.69	10.0	2.1	5.5
AJ	5:26:56	5:39:49	0:12:53	18.01	12.8	2.5	1.9
AK	5:39:49	5:56:57	0:17:08	23.36	15.5	5.9	3.4
AL	6:05:32	6:18:24	0:12:52	17.68	8.1	4.2	2.5

* Denotes straight-line distance between start and end points—does not account for variations in translation.

**Mesovortices denoted with maximum depth "N/A" featured scans where the mesovortex extended to the top of the radar volume or where considerable uncertainty was noted in the depth analysis

at 0255 UTC. By 0257 UTC, "E" had slowed considerably in forward motion, while to its south "F" accelerated. After 0257 UTC, "E" turned to the right (southeast), while "F" turned to the left, moving ahead of "E" by 0259 UTC and merging with "E" by 0300 UTC (Fig. 8). The overall behavior of the two mesovortices

resembles the behavior documented by Fujiwhara (1931), in which two vortices of nearly equal intensity were observed to have influenced each other's motion, inducing revolution around a center point, until the two vortices eventually merged.
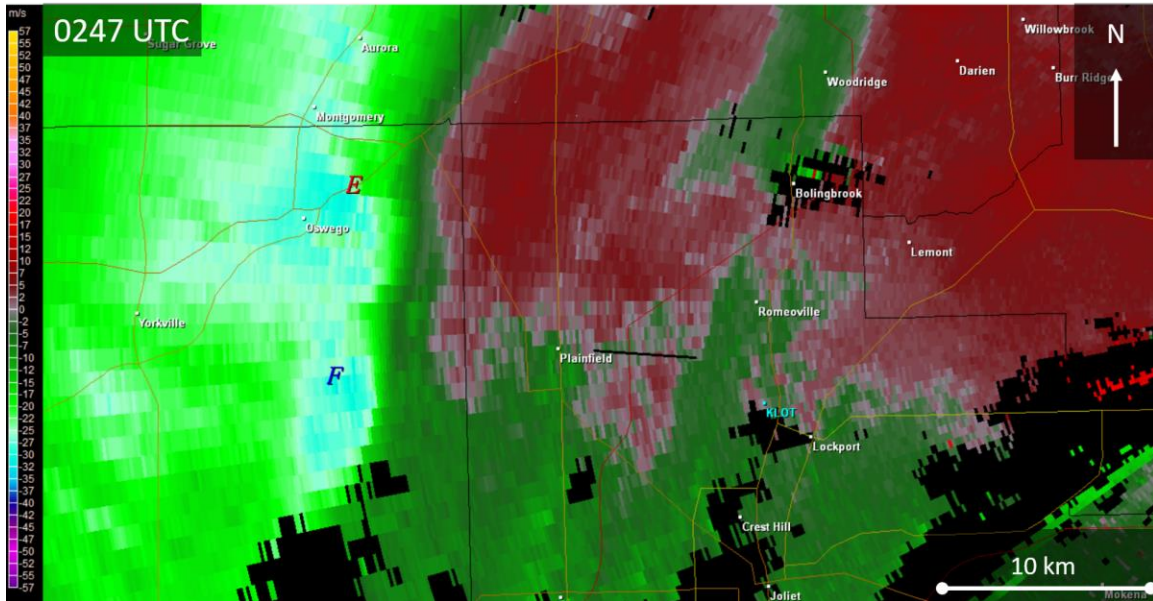
Figure 7: Loop of 0.3° plan position indicator (PPI) scans of radial velocity (V_r) from TMDW, 0247–0304 UTC 1 July 2014, illustrating the binary interaction between mesovortices "E" and "F". The solid black line represents the path of an EF1 tornado with "F". The average location of "E" and "F" from TMDW at 0247 UTC is 50 km at 270° and "E" is 27 km at 267° from TMDW at 0304 UTC. *Click image to enlarge and animate.*
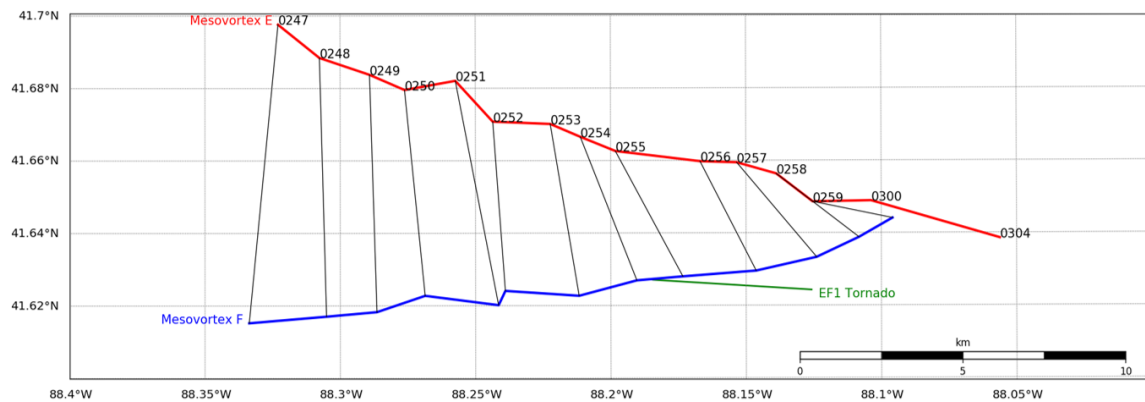
Figure 8: Plot of the positions of mesovortices "E" (red) and "F" (blue) from 0247–0304 UTC 1 July 2014. Black lines connect the locations of "E" and "F" at the same scan time. *Click image to enlarge.*
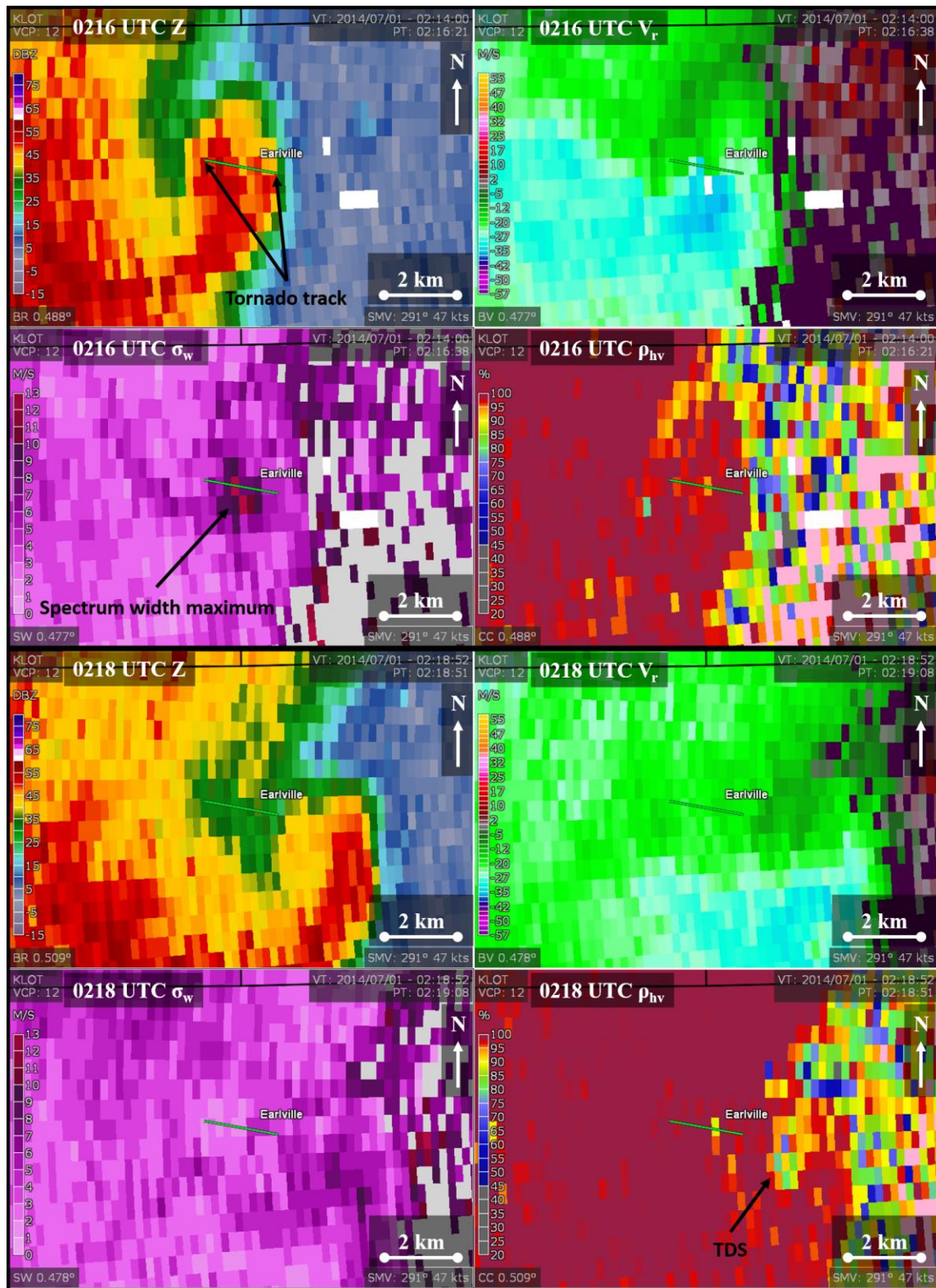
Figure 9: Four-panel 0.5°-elevation PPI images of reflectivity factor (*Z*), radial velocity (V$_r$), spectrum width (σ$_w$), and cross-polar correlation coefficient (ρ$_{hv}$) at 0216 UTC (top) and 0218 UTC (bottom) 1 July 2014 from KLOT, showing the evolution of mesovortex "B" during the Earlville, IL, tornado. "B" is located 69 km at 267° from KLOT at this time. *Click image to enlarge.*
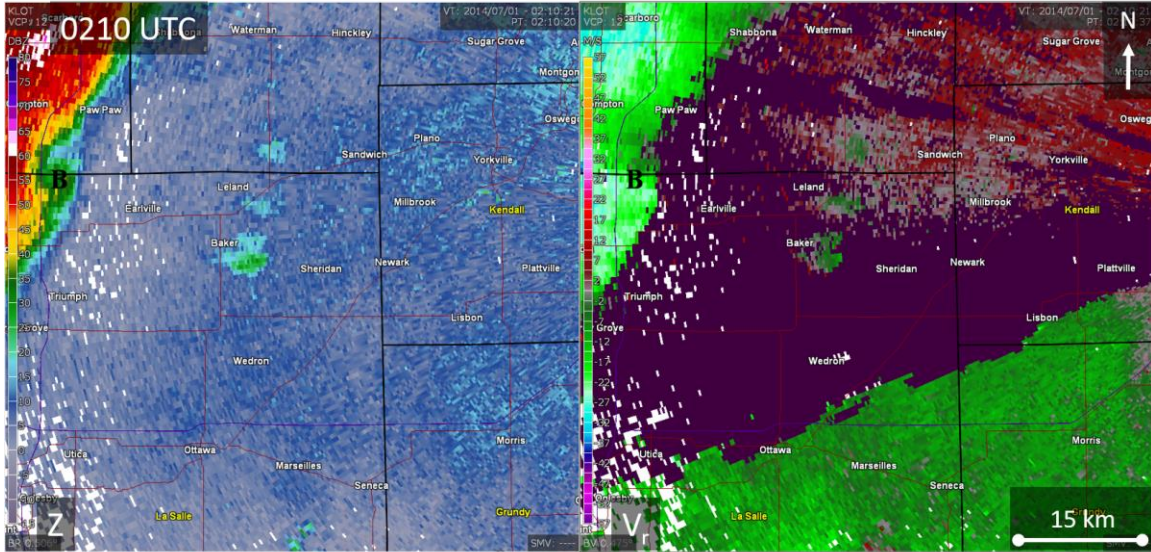
Figure 10: Two-panel PPI loop of Z and V$_r$ from 0210–0248 UTC 1 July 2014 from KLOT, showing the evolution of mesovortices "B", "C", and "D" and the beginning of "G". "B" is located 79 km at 272° from KLOT at 0210 UTC, and "G" is located 35 km at 229° from KLOT at 0248 UTC. *Click image to enlarge and animate.*
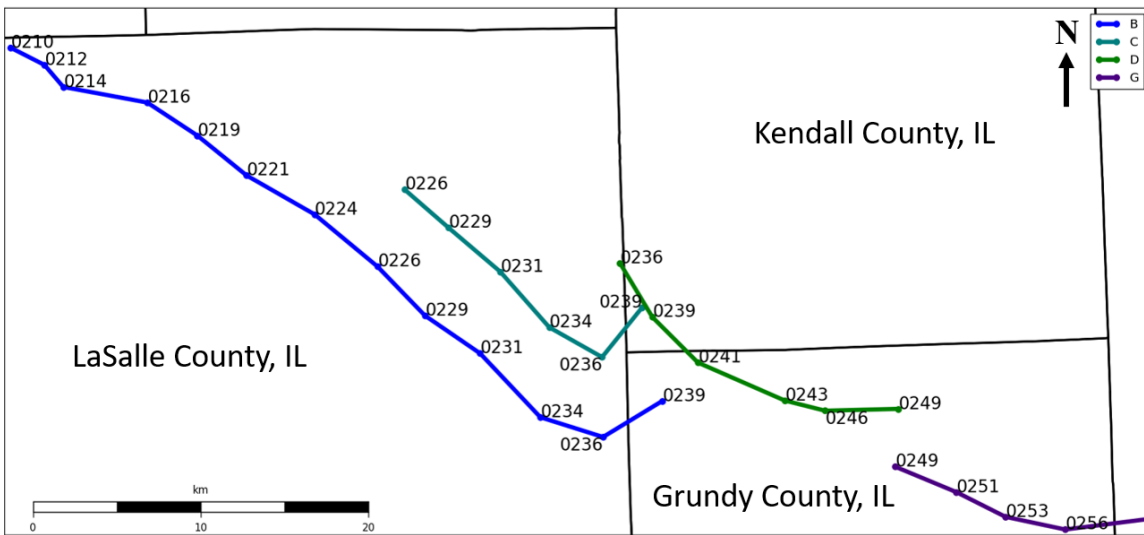

Figure 11: Path overview of mesovortices "B", "C", "D", and the start of "G". Numbers indicate time (UTC) of couplet location.

QLCS appeared to play a key role in the influenced each other's motion, inducing revolution around a center point, until the two vortices eventually merged.

b. The evolution of mesovortex "G"

1) The early development of mesovortex "G"

The most noteworthy feature of the second derecho was a large, long-lived mesovortex that developed across northeastern Illinois and moved into northern Indiana. This mesovortex, named "G", produced 14 of the 29 confirmed tornadoes from the event. It also produced widespread damage from winds estimated as high as 49 m s^{-1} (110 mph). Mesovortex "G" appeared to develop through a complex interaction of several mesovortices across north-central and

northeastern Illinois. The first mesovortex ("B") developed in north-central Illinois, where it produced an EF1 tornado near Earlville at 0216 UTC, the first confirmed tornado of the event (Fig. 9). As "B" propagated southeastward, a second mesovortex ("C") formed ≈4.9 km north-northeast of mesovortex "B" at 0226 UTC. A third mesovortex ("D") formed ≈5.7 km north of "C" at about 0236 UTC and traveled southeast, absorbing "B" and "C" while growing in size and intensity (Figs. 10 and 11). An EF1 tornado formed immediately after the merger of "C" into "D" at 0238 UTC.

Whether or not mesovortex "D" was directly involved in the intensification of the entity identified as "G" is unclear. Radar data from KLOT and damage survey results from an EF0 tornado in northern Grundy County indicate that mesovortex "D" turned toward the east. At the same time, a larger circulation quickly developed immediately to its south, producing widespread wind damage in the city of Morris (Fig. 10). This larger mesovortex ("G") grew in diameter from ≈6 km at 0246 UTC to ≈9 km by 0316 UTC. At 0319 UTC, a pair of subvortices began to appear within the broader mesovortex "G" structure. Both quickly became tornadic: the northern "G-1" at 0325 UTC, and the southern "G-2" at 0329 UTC (Fig. 12). The split of G into subvortices "G-1" and "G-2" is detailed in the following section.

2) Characteristics and behavior of subvortices "G-1" and "G-2"

Despite their development out of the broader circulation of mesovortex "G", the structure and evolution of "G-1" and "G-2" displayed marked differences. Initially they were of nearly equal intensity based on V_{ROT}, with "G-1" at 29.2 m s^{-1} and "G-2" at 26.4 m s^{-1}, a difference of only 2.8 m s^{-1} (Fig. 13a). With the exception of a substantial dip for "G-2" at 0325 UTC, their rotational velocities remained within 3.1 m s^{-1} of each other until about 0338 UTC. By 0343 UTC, the difference in V_{ROT} increased to 13.3 m s^{-1} (29.2 m s^{-1} for "G-1" and 15.9 m s^{-1} for "G-2"). This indicates the spread in intensity can be attributed both to a reintensification of "G-1" and a weakening of "G-2" (Fig. 13).

Substantial differences also can be found in the depths of subvortices "G-1" and "G-2". Immediately following the split, "G-1" was detectable to a depth of 6.1 km, while "G-2" was only detectable to a depth of 2.3 km. Subvortex "G-1" continued to deepen, with a maximum depth of 8.8 km reached at 0341 UTC, the maximum depth of any mesovortex observed during this event (see section 5). The depth of "G-1" decreased after this time, but never below the initial 6.1-km value. Meanwhile, "G-2" also deepened after the split, but only reached a peak depth of 3.6 km at 0346 UTC.
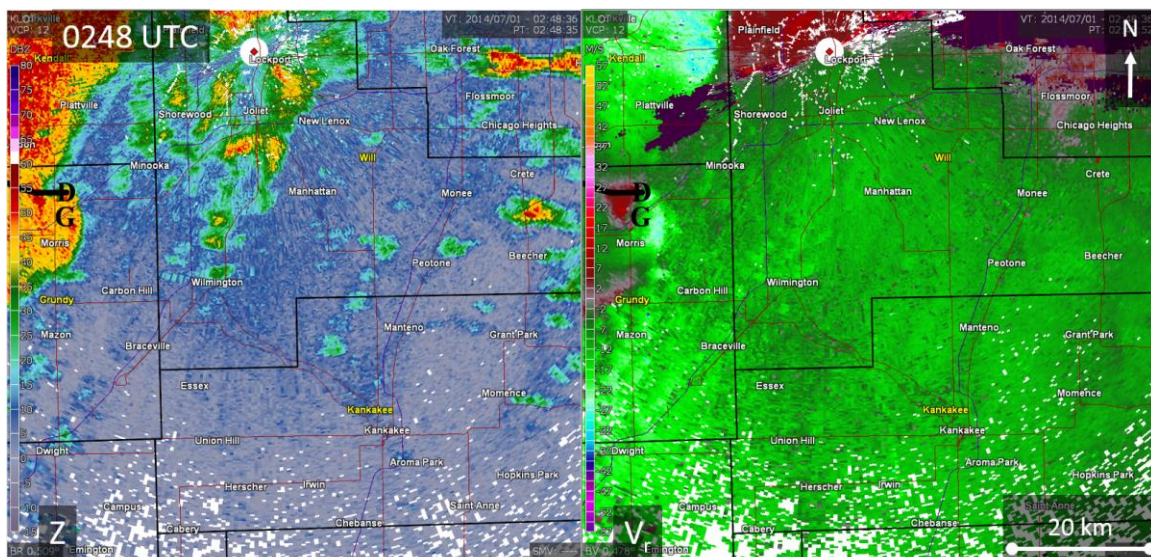
Figure 12: As in Fig. 10, but from 0248 UTC to 0330 UTC, showing the evolution of mesovortex "G" and its split into "G-1" and "G-2". "G" is located 35 km at 229° from KLOT at 0248 UTC, and "G-2" is located 59 km at 140° from KLOT at 0330 UTC. *Click image to enlarge and animate.*

a)

b)

c)

d)
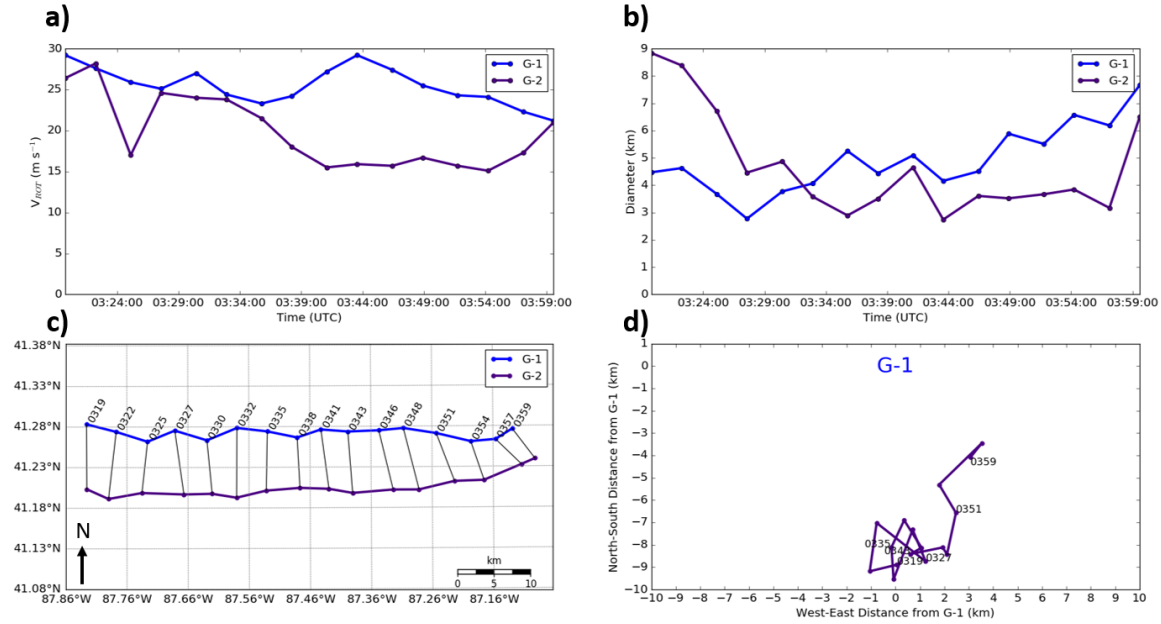
Figure 13: a) V_{ROT} time series; b) diameter; and c) track and location of subvortices "G-1" and "G-2". d) Location of subvortex "G-2" relative to subvortex "G-1". *Click image to enlarge.*

In addition to the larger intensity, size, and depth characteristics of "G-1" relative to "G-2", "G-1" may have directly influenced the evolution of "G-2" in the latter portion of their split lifecycles. Figures 13(c,d) depict their relative positions over the lifespans of the two subvortices.   Between 0319–0341 UTC, no discernable pattern is noticeable in the motion of "G-2" relative to "G-1", with only minor differences in position likely attributable to noise in the detection of their center locations. However, beginning at 0341 UTC, a notable acceleration of "G-2" relative to "G-1" is evident, with "G-2" moving around "G-1" counterclockwise.   Subvortex "G-1" absorbed "G-2" at 0359 UTC.

3) Breakdown of "G" into numerous smaller, cyclic mesovortices

The recombined mesovortex "G" slowly lost definition as it moved across northwestern Indiana, losing its identity after 0422 UTC. As the associated line segment moved eastward, several rapidly evolving mesovortices were observed: "P", "Q", "R", "T", "Z", "AA", and "AB" (Fig. 14). Mesovortices "P", "Q", and "R" each were detected first on the KIWX radar at 0435 UTC (Fig. 15) in southwestern Marshall and northwestern Fulton Counties, IN. Mesovortex "P" followed an east-southeast

trajectory (from ≈290°) during its brief lifespan and dissipated before 0444 UTC.

Farther to the south, "Q" and "R" featured eastward to east-northeastward motion (from ≈240–270°), each turning eastward near the end of its lifecycle. Mesovortex "Q" dissipated before 0456 UTC and "R" dissipated before 0501 UTC. Although no tornadoes were confirmed, possible or likely TDSs occurred with these mesovortices (Fig. 16). A survey from the Northern Indiana NWS office (including coauthor E. Bentley) found substantial damage with "R" but could not determine a definitive cause, and thus did not document it as a tornado in *Storm Data*.

After the formation of "P", "Q", and "R", mesovortex "T" developed to the south of "R" by 0439 UTC. This mesovortex "T" remained quite weak (V_{ROT} <10 m s^{-1}) until 0452 UTC when its V_{ROT} increased to 13.0 m s^{-1}. The subsequent 0.5° scan from KIWX (0456 UTC) revealed a TDS with "T", along with a substantial weakening of its V_{ROT} to ≈4.3 m s^{-1}. While the V_{ROT} of "T" briefly increased back to 9.9 m s^{-1} and ρ_{hv} within the original TDS region of mesovortex "T" dropped again from 0.77 at 0456 UTC down to 0.57 at 0501 UTC (Fig. 15), the associated velocity signature weakened by 0501 UTC, indicating the likelihood that any tornadic vortex had dissipated by that time.
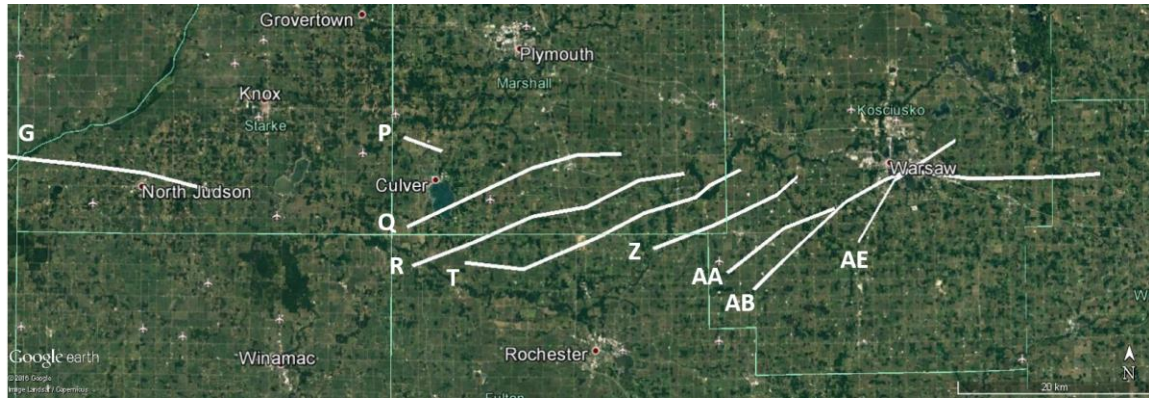
Figure 14: Overview map showing the demise of mesovortex "G" and the locations of mesovortices "P", "Q", "R", "T", "Z", "AA", "AB", and "AE". Background image from GoogleEarth®. *Click image to enlarge.*
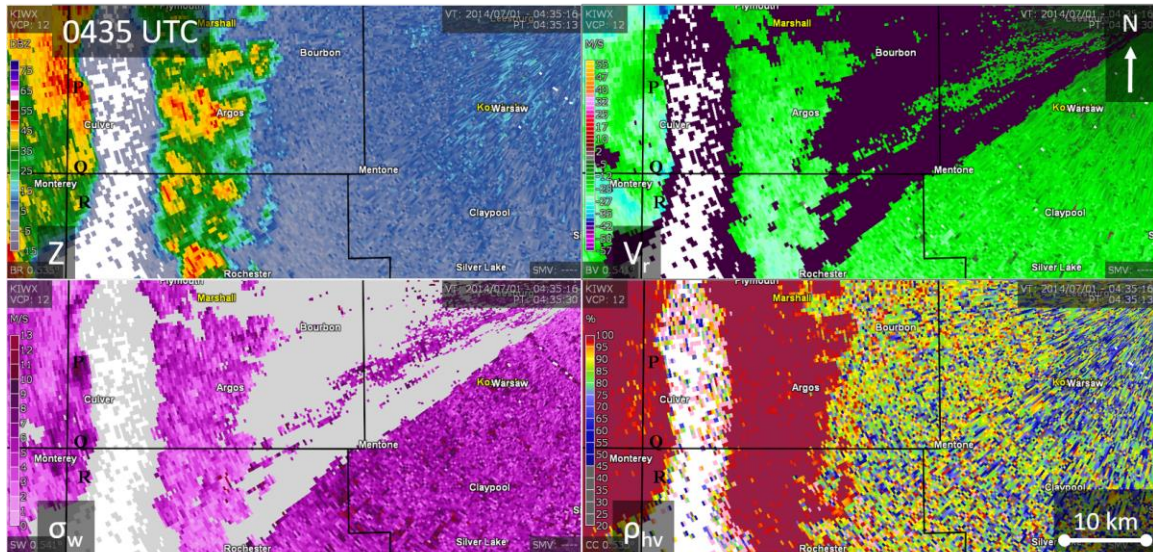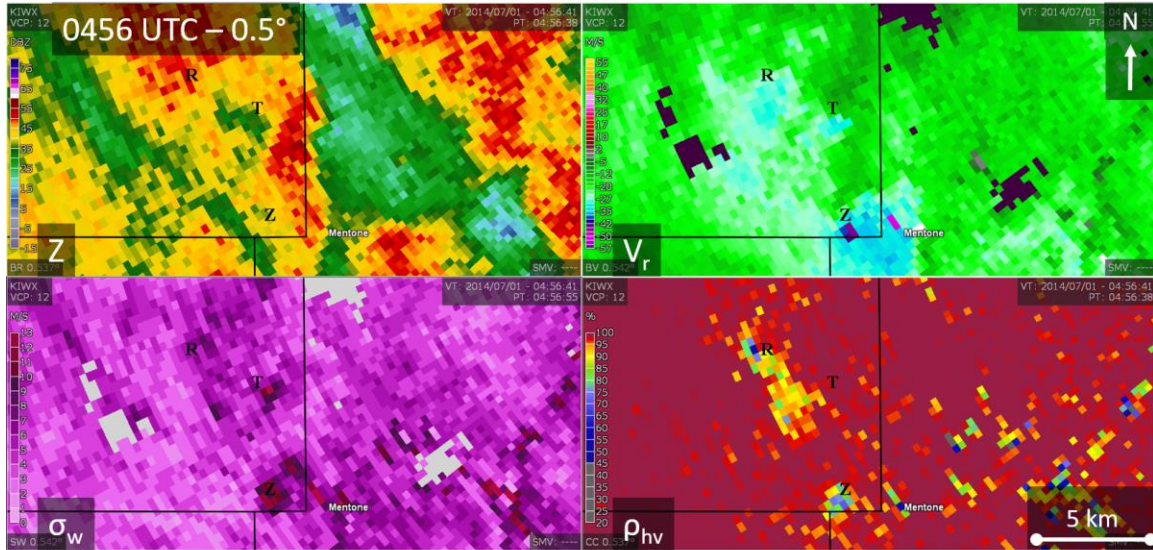

Figure 15: Four-panel 0.5°-elevation PPI loop of Z, V_r, σ_w, and ρ_{hv} from 0435–0505 UTC 1 July 2014, from KIWX, showing the evolution of mesovortices "P", "Q", "R", "T", "Z", "AA", "AB", and "AE". "P" is located 64 km at 260° from KIWX at 0435 UTC, and "AB" is located 25 km at 225° from KIWX at 0505 UTC. *Click image to enlarge and animate.*

As mesovortex "Q" dissipated and "R" and "T" were ongoing, "Z" formed ≈3.8 km to the south-southeast of "T" around 0452 UTC. A TDS quickly developed in association with "Z" by 0456 UTC as its V_{ROT} reached a maximum of 14.7 m s^{-1}. While "Z" reached peak intensity, two additional weak circulations formed to its southeast: "AA" and "AB" at distances of ≈5.1 and ≈7.8 km respectively.

At 0501 UTC, mesovortex "Z" still maintained a well-defined circulation in Doppler velocity, but its TDS began to merge with the

lower ρ_{hv} associated with "R", and "T", likely due to the dispersion of tornado debris (Van Den Broeke 2015). Mesovortices "AA" and "AB" were both more intense at 0501 UTC than at 0456 UTC, with V_{ROT} values of 9.5 m s^{-1} and 9.7 m s^{-1}, respectively. In addition to their strengthening, "AA" and "AB" moved closer to each other, with a distance of ≈2.4 km between their center points. By 0505 UTC, "Z" had almost dissipated, with a V_{ROT} of only 7.5 m s^{-1}. Meanwhile, the identities of "AA" and "AB" were nearly indistinguishable at this time, with the two mesovortices likely in the process of

15

<u>Figure 16</u>: Four-panel PPI loop of Z, V_r, σ_w, and ρ_{hv} as labeled, from 0.5°–3.1° elevation at 0456 UTC 1 July 2014 from KIWX, showing the vertical continuity of the TDSs associated with mesovortices "R", "T", and "Z". The TDSs with "R" and "T" extend to 1.4° using a threshold of ρ_{hv} <0.9 (Clayton et al. 2016, Skow and Cogil 2017) before being contaminated by Z <30 dBZ, while the TDS with "Z" extends to ρ_{hv} <1.9° until values become unsupportive of debris. "Z" is located 37 km at 238° from KIWX at 0.5°. *Click image to enlarge and animate.*

merging into one (Fig. 15). A tornado was confirmed near the vicinity of "AA" and "AB" at this time, with a path orientation from northwest to southeast. This orientation was nearly 90° perpendicular to the mean motion of the two mesovortices, potentially indicating that either: 1) "AA" revolved around "AB" during their merger (Fig. 17), or 2) the tornado revolved around the center of "AB". Eventually, "AB" turned to the east and dissipated after 0526 UTC.

As mesovortices "Q" through "AB" evolved within the main QLCS, a secondary line of convection formed ahead of the main system (Fig. 15). As "AA" and "AB" intensified, this new leading band of convection developed its own mesovortex ("AE") at 0501 UTC directly east of "AA" and "AB", at distances of 7.8 km and 6.6 km, respectively (Fig. 15). Mesovortex "AE" reached a peak V_{ROT} of 14.8 m s^{-1} at 0505 UTC before crossing the eventual path of "AB" and dissipating after 0509 UTC. After "AE" and "AB" dissipated, the main QLCS and leading convective band merged into one convective line segment and produced two additional mesovortices ("AJ" and "AK") before the line weakened in northwestern Ohio (not shown).

c. Evidence of satellite behavior in mesovortices

As previously discussed, the number of simultaneously occurring mesovortices observed in the second QLCS increased dramatically across northwestern and north-central Indiana relative to the mesovortices documented in northern Illinois. This dramatic increase in the number of mesovortices created the opportunity for complex interactions between them. One of the most remarkable was the satellite behavior of three mesovortices around a larger, long-lived mesovortex.

Mesovortex "K" was long-lived, first appearing at 0404 UTC just east of Valparaiso in Porter County, IN, then dissipating after 0522 UTC just west of Topeka in LaGrange County, IN, for a total distance traveled of 113 km over 78 min (Fig. 18). "K" was responsible for a pair of EF1 tornadoes at South Center and Koontz Lake (not shown). As "K" moved eastward across northern Indiana, a weak mesovortex ("U") developed at around 0444 UTC at a distance of≈6.6 km south of "K". By 0448 UTC, "U" had advanced ahead of "K", about 5.3 km to its east- southeast. In addition to the advancement of "U", two additional
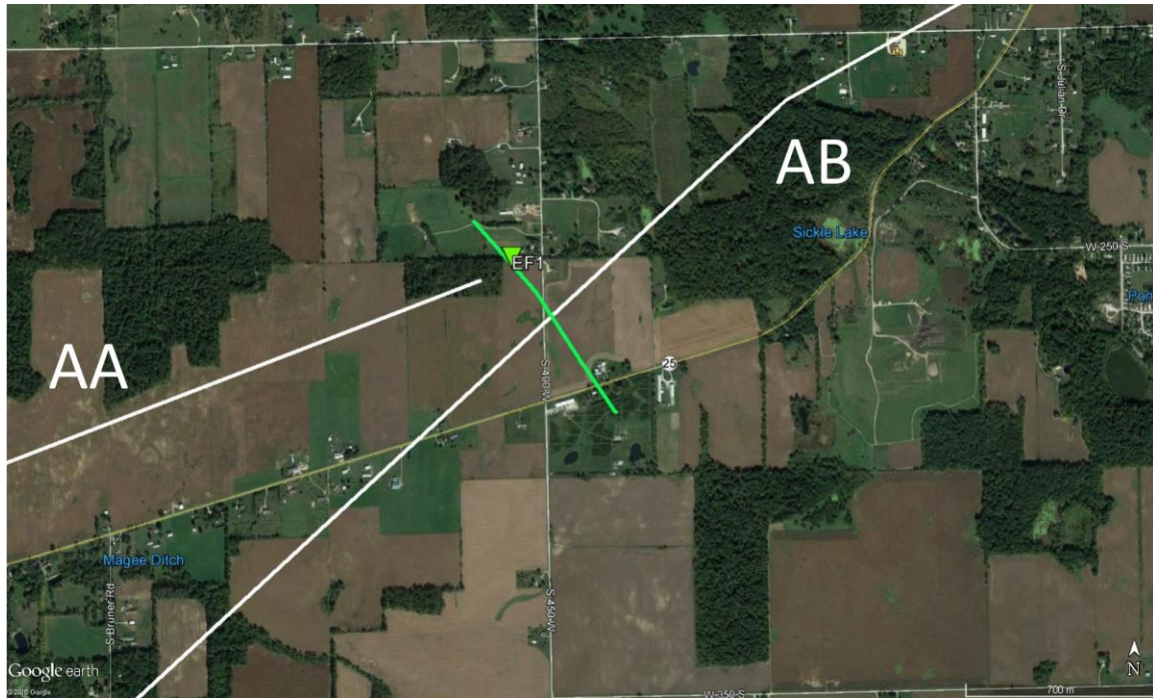
Figure 17: Overview map of the paths of mesovortices "AA" and "AB" in relation to the Gravelton, Indiana EF1 tornado on 1 July 2014. Background image from GoogleEarth®. *Click image to enlarge.*

("V" and "W") became apparent from KIWX radar. Mesovortex "V" was located approximately 5.0 km northeast of "K", while "W" was located at around 6.1 km south of "K", a very similar location to the genesis location of "U" relative to "K".

At 0452 UTC, "U" was located ≈3.0 km east of "K", while "V" was 2.8 km northeast of "K", and "W" was 3.3 km south-southeast of "K". Mesovortices "U" and "V" were detected last at 0456 UTC, with "U" located ≈1.7 km northeast of "K" (possibly being absorbed into the larger circulation of mesovortex "K") and mesovortex "V" located at around 3.3 km north of "K". While "U" and "V" were moving toward and possibly being absorbed into "K" at 0456 UTC, "W" also was still ongoing 2.0 km southeast of "K". Mesovortex "W" was detected last on KIWX at 0501 UTC, about 3.0 km south of "K" (Fig. 19).

Mesovortices "U", "V", and "W" each displayed satellite behavior similar to that displayed in some tornadoes (Fig. 20; Wurman and Kosiba 2013; Edwards 2014). The behavior of "U", "V", and "W" closely resembled the conceptual schematic for satellite tornadoes provided in Edwards (2014), in which the satellite tornado not only revolves around the main tornado, but is also drawn inward toward it before the satellite vortex either dissipates or merges with the main tornado. This behavior can be seen in "U", "V", and "W", where the bearings all shift in a counterclockwise direction as the distances between the three mesovortices and the parent mesovortex "K" decrease. Because of the low temporal resolution provided by the KIWX radar, no definitive determination could be made as to whether mesovortices "U", "V", and "W" merged with mesovortex "K" or dissipated before merger, although it appears from the 0456 UTC volume that the demise of "U" may have been via merger with "K".

5. Analysis and discussion

The mesovortices of 30 June–1 July 2014 across northern Illinois and northern Indiana displayed a remarkable array of characteristics and behaviors. These included a binary (Fujiwhara 1931) interaction, splitting and re-merging of a large mesovortex, and satellite behavior of mesovortices around a larger mesovortex. An additional analysis of the general characteristics of nontornadic and tornadic mesovortices and their behaviors and

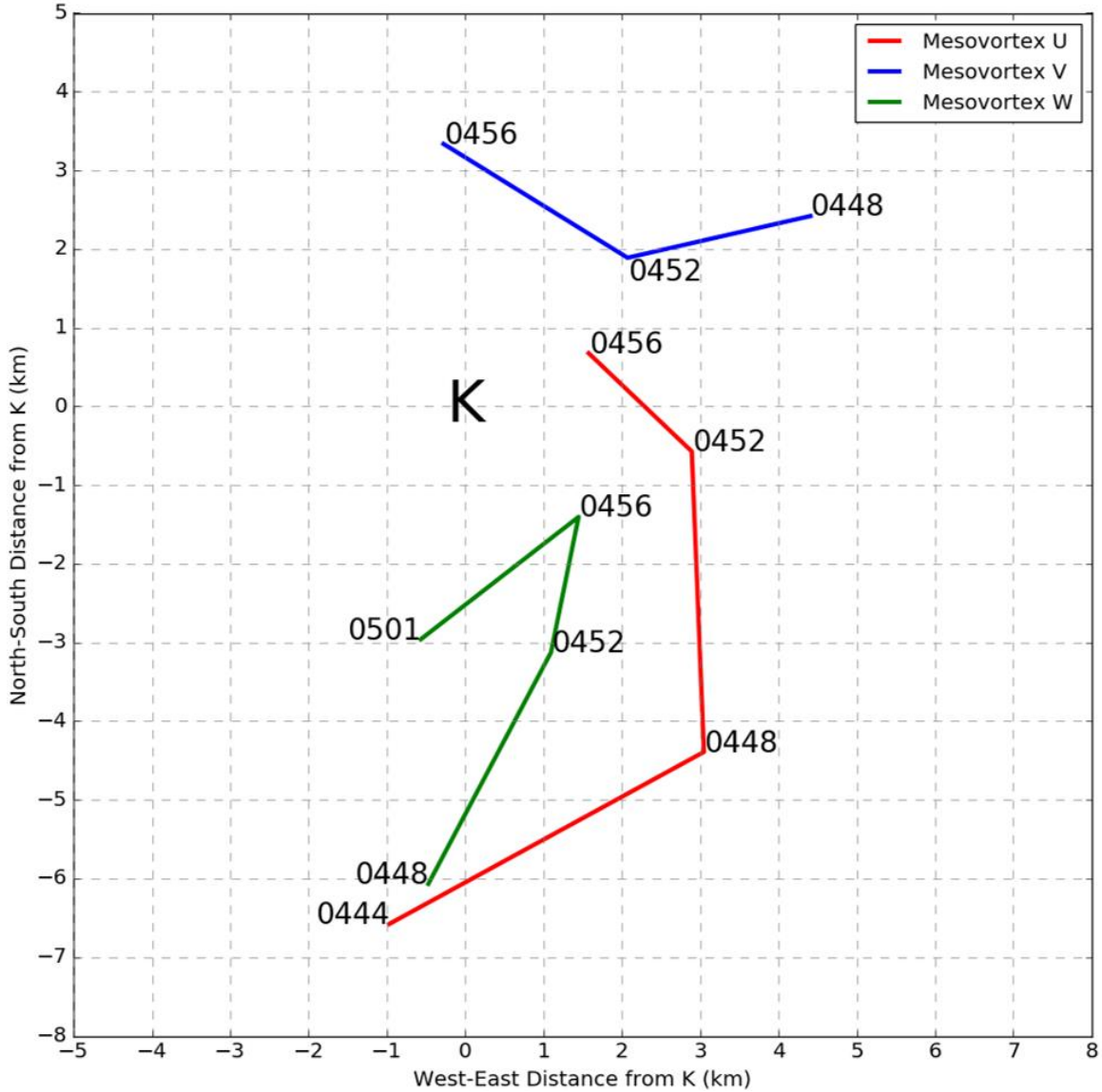Figure 18: Overview map of mesovortices "K", "U", "V", and "W" across northern Indiana. *Click image to enlarge.*
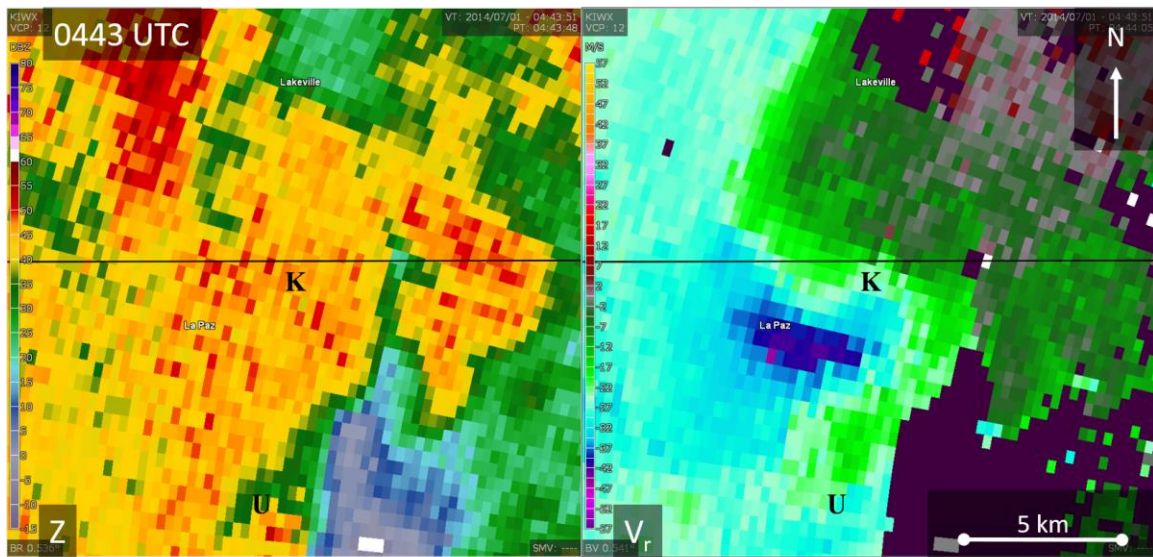
Figure 19: Two-panel storm-following PPI loop of Z and radial velocity (V$_r$) from 0443–0501 UTC 1 July 2014 from KIWX, centered on mesovortex "K", showing the revolution of "U", "V", and "W" around "K". "K" is located 50 km at 285° from KIWX at 0443 UTC and 29 km at 305° from KIWX at 0501 UTC. *Click image to enlarge and animate.*

characteristics was undertaken to ascertain their likely generation mechanisms.

None of the data evaluated showed statistically significant differences between confirmed-tornadic, possibly tornadic, or nontornadic mesovortices (Figs. 21–26). While mesovortices with confirmed tornadoes tended to be larger, deeper, stronger, and more persistent than their nontornadic counterparts, the possibly tornadic mesovortices tended to be smaller, more transient, shallower, and somewhat weaker than both their confirmed-tornadic and nontornadic counterparts. This seeming anomaly was driven largely by a series of rapidly cycling mesovortices (mesovortices "R", "T", and "Z") that originated in the remnant enhanced shear zone from a much larger dissipated mesovortex

(mesovortex "G"). Each of these mesovortices was near the KIWX radar, sampled at close range, and showed a clear TDS (section 4b). These rapidly evolving vortices, in addition to the short-lived mesovortices "H", "V", and "AL", substantially lower the average duration and size of the combined "possibly tornadic" and "confirmed-tornadic" mesovortices. The lack of damage surveys performed on the "possibly tornadic" mesovortices does cast uncertainty on their true nature. However, the majority of these "possibly tornadic vortices" ("E", "R", "T", "V", "Z", "AB", "AJ", and "AL") showed suspected or likely TDSs and tight rotational couplets, while "H" showed a tight couplet and evidence of convergent tree damage in satellite imagery gathered after the event.

Figure 20: Overview map of the paths of "U", "V", and "W" with respect to the location of mesovortex "K", showing the tendency for "U", "V", and "W" to revolve around "K".

All vortices in this study were noted to be rotating cyclonically, with no anticyclonic mesovortices observed. Trapp and Weisman (2003) detailed two potential processes for mesovortex genesis, each focusing on the downward tilting of horizontal vorticity. In their early-stage hypothesis, convective downdrafts are responsible for the downward tilting of horizontal vorticity generated by the buoyancy gradient and resulting baroclinicity along the gust front, while the mature–late stage mesovortices form via downward tilting of horizontal vorticity generated by intense vertical shear underneath the RIJ. In the early stage

hypothesis, the cyclonic mesovortex forms on the right and the anticyclonic vortex forms on the left along a plane normal to the forward motion vector of the QLCS, while the opposite is true for the RIJ hypothesis.

Atkins and St. Laurent (2009b) also present two hypotheses for mesovortex genesis, both involving upward tilting of horizontal vorticity. The first hypothesis explains the development of cyclonic-only mesovortices through upward tilting of streamwise vorticity generated by both environmental shear and gust-front baroclinicity during all stages of QLCS development. The
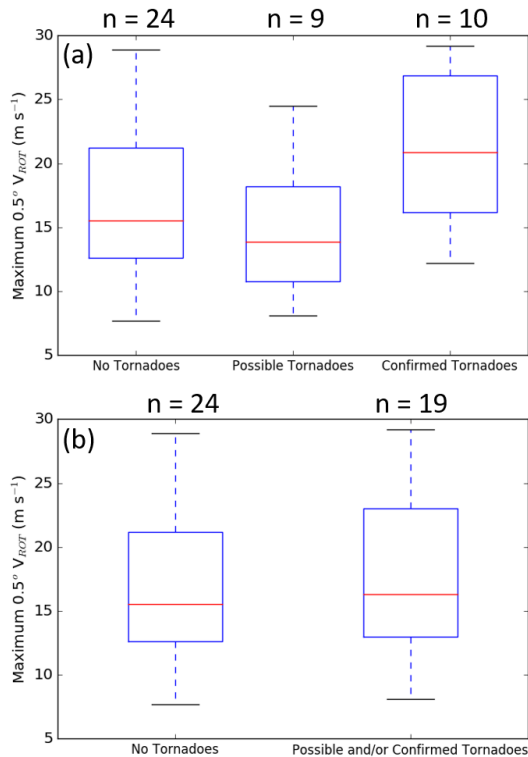
Figure 21: Box plots of maximum 0.5° V$_{ROT}$ for a) nontornadic, possibly tornadic, and confirmed-tornadic mesovortices, and b) nontornadic and combined possibly tornadic and confirmed tornadic mesovortices. The number of mesovortices that fill each category are listed atop each plot. (Note: The total number of mesovortices adds up to 43 due to the splitting of mesovortex "G" into 6 different parts. See Table 1 and Section 4b for more details.) The boxes indicate the middle 50% of data, and the whiskers indicate either the maximum/minimum data values or the ends of the boxes ±- 1.5 times the interquartile range. *Click image to enlarge.*

second hypothesis explains the development of cyclonic/anticyclonic mesovortex couplets through upward tilting of vorticity generated by gust-front baroclinicity, with a cyclonic vortex on the left and anticyclonic vortex on the right along a plane normal to the motion of the gust front. Observations of a bow echo from the Bow Echo and Mesovortex Experiment (BAMEX; Davis et al. 2004) appear to support the Trapp and Weisman hypothesis for downward tilting of baroclinically-generated vorticity, albeit with a different downdraft source (Wakimoto et al. 2006b). Wheatley and Trapp (2008) also identified the Trapp and Weisman (2003) mechanism in numerical simulations of the
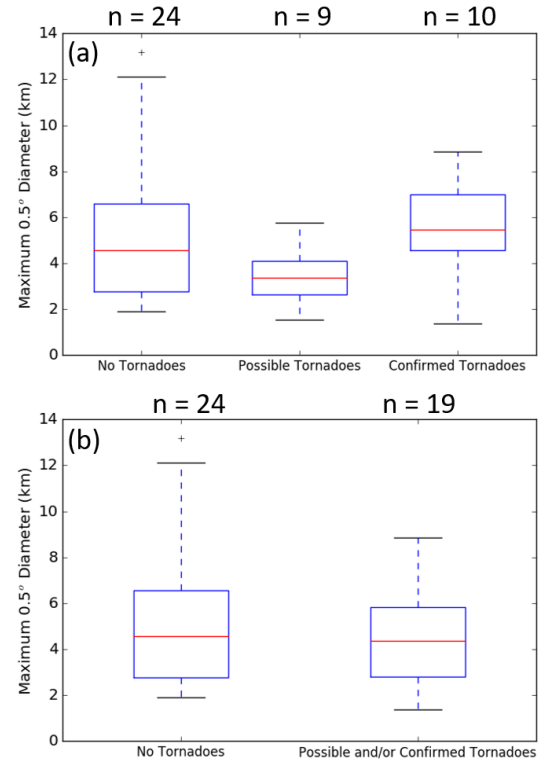

Figure 22: As in Fig. 21 but for maximum 0.5° diameter of observed mesovortices. *Click image to enlarge.*

Wakimoto et al. (2006b) case, but found the release of horizontal shearing instability along a vortex sheet and subsequent stretching by updrafts to be the main cause of mesovortex genesis in a simulated cold season case.

The lack of anticyclonic vortices observed in the present case would seem to exclude mesovortex generation mechanisms that rely upon either the upward or downward tilting of crosswise vorticity, such as those processes described in Trapp and Weisman (2003) and in early-stage cases in Atkins and St. Laurent (2009b). Instead, the more likely causes of mesovortex generation involve either streamwise vorticity tilting generated by environmental shear and/or baroclinicity along the gust front (e.g., Atkins and St. Laurent 2009b) or through the release of horizontal shearing instability (e.g Wheatley and Trapp 2008).

The three-dimensionality of the behaviors observed during the second 30 June–1 July 2014 QLCS, particularly the satellite mesovortices and mesovortex generation and motion, casts doubt on the role of shearing instability in the generation
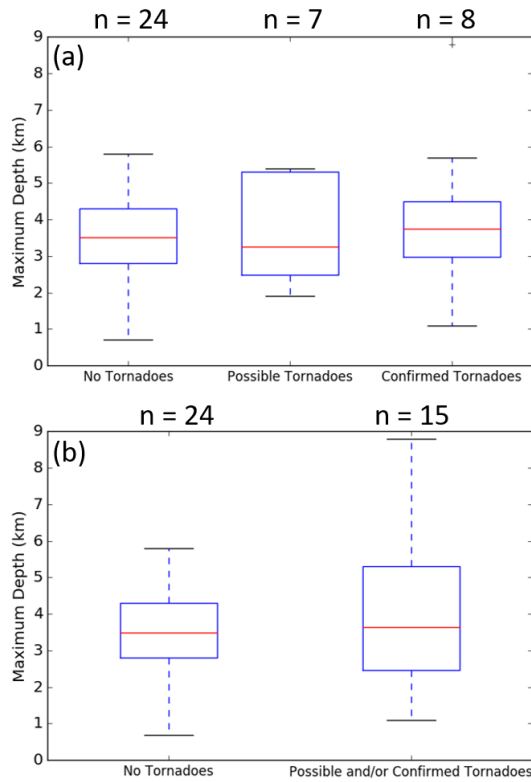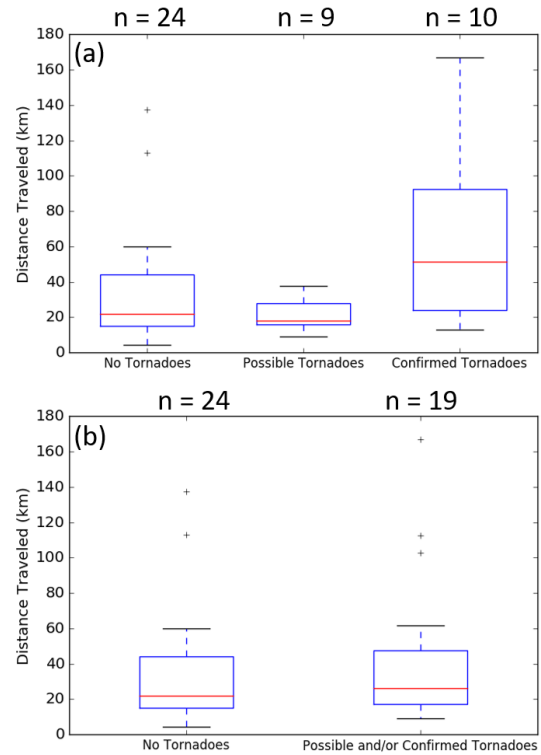
Figure 23: As in Fig. 21, but for the maximum depth of observed mesovortices. *Click image to enlarge.* (Note: The numbers of sampled mesovortex maximum depths for confirmed-tornadic and possibly tornadic mesovortices is less than for the other characteristics due to uncertainties in the maximum depths of "E", "F", "M", and "AB".)

Figure 24: As in Fig. 21, but for distance traveled of each observed mesovortex. *Click image to enlarge.*

of many of these vortices. This is consistent with the findings of Trapp and Weisman (2003) and Atkins and St. Laurent (2009b), as well as the warm-season case detailed in Wheatley and Trapp (2008). However, the very even spacing of mesovortices "Q", "R", "T", and "Z" in particular suggest that horizontal shearing instability cannot be discounted completely as a possible genesis mechanism. It is likely that in this case (and other QLCS cases), multiple genesis mechanisms may be at work to produce the observed mesovortices.

6. Summary and conclusions

A pair of tornadic QLCSs impacted the upper Mississippi River Valley and southern Great Lakes region between the midday hours of 30 June and the overnight hours of 1 July 2014.

The first QLCS developed across eastern Nebraska and Iowa, producing 11 tornadoes during the afternoon before weakening across the southern Great Lakes during the early evening. The second QLCS, which developed only 250 km behind and <3 h after the first, was notable in several respects. It produced a prolific number of leading-edge mesovortices (38) and 29 confirmed tornadoes, despite following the first tornado-producing QLCS that had passed over the affected areas. Numerous unconfirmed tornadoes also are suspected, based on radar and high-resolution satellite imagery across northern Illinois and northern Indiana. This study has sought to shed additional light on the most likely mechanisms governing the generation and evolution of these mesovortices. The more rapid low-level scanning of mesovortices using the SAILS algorithm, the addition of polarimetric radar technology, and the passage of the QLCS near two WSR-88Ds and one terminal Doppler radar site, led to these observations of intriguing behaviors and interactions with the mesovortices associated with the line:
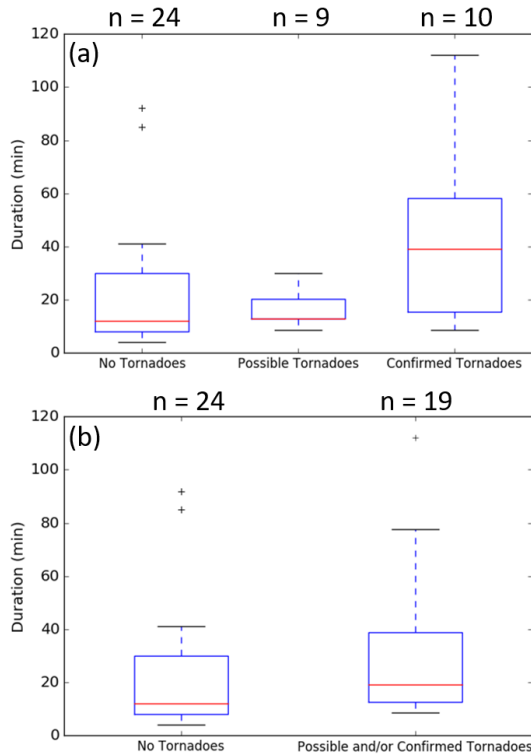
Figure 25: As in Fig. 21, but for duration of observed mesovortices. *Click image to enlarge.*

1) Multiple successive mesovortex mergers;

2) The splitting of a very large mesovortex into two prolifically tornadic subvortices;

3) A binary (Fujiwhara) interaction between two mesovortices;

4) Rapid, successive evolution of numerous tornadic or potentially-tornadic mesovortices in a cyclic fashion;

5) The merging of numerous TDS signatures into one large ρ_{hv} depression;

6) The formation of a mesovortex within a secondary, leading convective band; and

7) Satellite behavior of three mesovortices around a larger, long-lived mesovortex.

It is not immediately clear how rare these interactions are in the context of all QLCSs. The recent implementation of SAILS and the newer MESO-SAILS technology (Chrisman 2014), to increase scanning frequency of the lowest elevations, also allows for more detailed observations of the low levels of convective storms, and future studies may reveal these types of behaviors to be fairly ubiquitous in severe QLCSs.
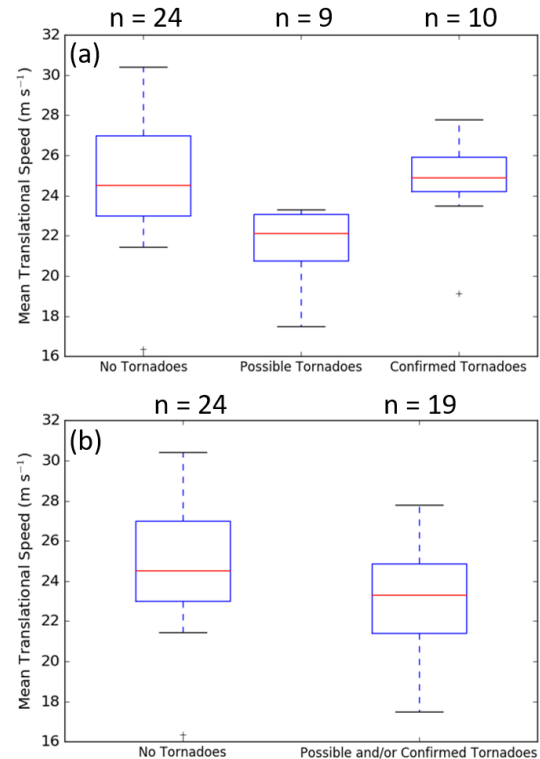
Figure 26: As in Fig. 21, but for mean translational speed of observed mesovortices. *Click image to enlarge.*

A collective analysis of the mesovortex characteristics revealed little difference between confirmed-tornadic, possibly tornadic, and nontornadic mesovortex characteristics, including maximum lowest-radar-tilt diameter, maximum depth, duration, and maximum intensity. This lack of distinction between tornadic and nontornadic mesovortices poses a particular challenge to warning forecasters trying to determine how to warn appropriately for such mesovortices based solely on their radar characteristics.

This case also raises questions about the generation mechanisms for mesovortices. The cyclonic-only nature of the mesovortices observed eliminates any mechanisms for generation that involve either upward or downward tilting of crosswise vorticity, while the three-dimensional nature of the mesovortex interactions casts doubt on any role of shearing instability in their generation. The upward tilting of streamwise vorticity appears the most likely cause of mesovortex generation in this case, but cannot be proven with the available dataset.

The second 30 June–1 July 2014 QLCS highlighted many challenges to the understanding of QLCS mesovortices. While challenges in detection, warning, and assessment of tornadoes formed by QLCS mesovortices are fairly universal, this event captured a complexity of mesovortex behavior not previously documented in the literature. Future analyses of tornadic QLCS events are encouraged in order to determine how common these complex behaviors and overarching mesovortex characteristics are, particularly in light of the aforementioned recent advancements in radar technology.

ACKNOWLEDGMENTS

REFERENCES

Arnott, N. R., Y. P. Richardson, J. M. Wurman, and E. N. Rasmussen, 2006: Relationship between a weakening cold front, misocyclones, and cloud development on 10 June 2002 during IHOP. *Mon. Wea. Rev.*, **134**, 311–335.

Atkins, N. T., J. M. Arnott, R. W. Przybylinski, R. A. Wolf, and B. D. Ketcham, 2004: Vortex structure and evolution within bow echoes. Part I: Single-Doppler and damage analysis of the 29 June 1998 derecho. *Mon. Wea. Rev.*, **132**, 2224–2242.

——, and C. S. Bouchard, R. W. Przybylinski, R. J. Trapp, and G. Schmocker, 2005: Damaging surface winds within the 10 June 2003 Saint Louis bow echo during BAMEX. *Mon. Wea. Rev.*, **133**, 2275–2296.

——, and M. St. Laurent, 2009a: Bow echo mesovortices, part I: Processes that influence their damaging potential. *Mon. Wea. Rev.*, **137**, 1497–1513.

——, and ——, 2009b: Bow echo mesovortices, part II: Their genesis. *Mon. Wea. Rev.*, **137**, 1514–1532.

Brotzge, J., and S. Erickson, 2009: NWS tornado warnings with zero or negative lead times. *Wea. Forecasting*, **24**, 140–154.

——, and ——, 2010: Tornadoes without NWS warning. *Wea. Forecasting*, **25**, 159–172.

——, S. E. Nelson, R. L. Thompson, and B. T. Smith, 2013: Tornado probability of detection and lead time as a function of convective mode and environmental parameters. *Wea. Forecasting*, **28**, 1261–1276.

Brown, R. A., L. R. Lemon, and D. W. Burgess, 1978: Tornado detection by pulsed Doppler radar. *Mon. Wea. Rev.*, **106**, 29–38.

Buban, M. S., and C. L. Ziegler, 2016: The formation of small-scale atmospheric vortices via baroclinic horizontal shearing instability. *J. Atmos. Sci.*, **73**, 2085–2104.

——, ——, E. N. Rasmussen, and Y. P. Richardson, 2007: The dryline on 22 May 2002 during IHOP: Ground radar and in situ data analyses of the dryline and boundary layer evolution. *Mon. Wea. Rev.*, **135**, 2473–2505.

Chrisman, J., 2014: Multiple Elevation Scan Option for SAILS (MESO-SAILS). NWS/Radar Operations Center, 27 pp. [Available online at https://www.roc.noaa.gov/WSR88D/PublicDocs/NewTechnology/MESO-SAILS_Description_Briefing_Jan_2014.pdf.]

Clayton, A. W., A. W. Lyza, R. Wade, and K. R. Knupp, 2016: An analysis of tornado debris signatures in the 30 June–1 July 2014 quasi-linear convective system tornado outbreak. Preprints, *28th Conf. on Severe Local Storms*, Portland, OR, Amer. Meteor. Soc., P1.12.

Coniglio, M. C., and D. J. Stensrud, 2004: Interpreting the climatology of derechos. *Wea. Forecasting*, **19**, 595–605.

Corfidi, S. F., M. C. Coniglio, A. E. Cohen, and C. M. Mead, 2016: A proposed revision to the definition of "derecho." *Bull. Amer. Meteor. Soc.*, **97**, 935–949.

Davis, C., and Coauthors, 2004: The Bow Echo and MCV Experiment: Observations and opportunities. *Bull. Amer. Meteor. Soc.*, **85**, 1075–1093.

Desrochers, P. R., and F. I. Harris, 1996: Interpretation of mesocyclone vorticity and divergence structure from single-Doppler radar. *J. Appl. Meteor.*, **35**, 2191–2209.

Edwards, R., 2014: Characteristics of supercellular satellite tornadoes. Preprints, 27th *Conf. on Severe Local Storms*, Madison, WI, Amer. Meteor. Soc., 17.5.

Forbes, G. S., and R. M. Wakimoto, 1983: A concentrated outbreak of tornadoes, downbursts and microbursts, and implications regarding vortex classification. *Mon. Wea. Rev.*, **111**, 220–235.

Friedlein, M., R. Castro, E. Lenning, A. W. Lyza, and K. R. Knupp, 2015: Evolution of the 30 June 2014 double derecho event in Northern Illinois & Northwest Indiana. Preprints, *27th Conf. on Weather Analysis and Forecasting*, Chicago, IL, Amer. Meteor. Soc.

Friedrich, K., D. E. Kingsmill, and C. R. Young, 2005: Misocyclone characteristics along Florida gust fronts during CaPE. *Mon. Wea. Rev.*, **133**, 3345–3367.

Fujita, T. T., 1978: Manual of downburst identification for project NIMROD. SMRP Res. Pap. 156, University of Chicago, 104 pp.

——, 1981: Tornadoes and downbursts in the context of generalized planetary scales. *J. Atmos. Sci.*, **38**, 1511–1534.

Fujiwhara, S., 1931: Short note on the behavior of two vortices. *Proc. Phys. Math. Soc. Japan*, *Ser. 3*, **13**, 106–110.

Funk, T. W., K. E. Darmofal, J. D. Kirkpatrick, V. L. Dewald, R. W. Przybylinski, G. K. Schmocker, and Y-J. Lin, 1999: Storm reflectivity and mesocyclone evolution associated with the 15 April 1994 squall line over Kentucky and southern Indiana. *Wea. Forecasting*, **14**, 976–993.

Guastini, C. T., and L. F. Bosart: 2016: Analysis of a progressive derecho climatology and associated formation environments. *Mon. Wea. Rev.*, **144**, 1363–1382.

Johns, R. H., and W. D. Hirt, 1987: Derechos: Widespread convectively induced windstorms. *Wea. Forecasting*, **2**, 32–49.

Knupp, K. R., and Coauthors, 2014: Meteorological overview of the devastating 27 April 2011 tornado outbreak. *Bull. Amer. Meteor. Soc.*, **95**, 1041–1062.

Lanicci, J. M., and T. T. Warner, 1991: A synoptic climatology of the elevated mixed-layer inversion over the southern Great Plains in spring. Part III: Relationship to severe-storms climatology. *Wea. Forecasting*, **6**, 198–213.

Lee, B. D., and R. B. Wilhelmson, 1997: The numerical simulation of non-supercell tornadogenesis. Part I: Initiation and evolution of pretornadic misocyclone circulations along a dry outflow boundary. *J. Atmos. Sci.*, **54**, 32–60.

Maddox, R. A., L. R. Hoxit, and C. F. Chappell, 1980: A study of tornadic thunderstorm interactions with thermal boundaries. *Mon. Wea. Rev.*, **108**, 322–336.

Markowski, P. M., E. N. Rasmussen, and J. M. Straka, 1998: The occurrence of tornadoes in supercells interacting with boundaries during VORTEX-95. *Wea. Forecasting*, **13**, 852–859.

Marquis, J., Y. P. Richardson, and J. M. Wurman, 2007: Kinematic observations of misocyclones along boundaries during IHOP. *Mon. Wea. Rev.*, **135**, 1749–1768.

Murphey, H. V., R. M. Wakimoto, C. Flamant, and D. E. Kingsmill, 2006: Dryline on 19 June 2002 during IHOP. Part I: Airborne Doppler and LEANDRE II analyses of the thin line structure and convection initiation. *Mon. Wea. Rev.*, **134**, 406–430.

NCEI, cited 2016: *Storm Data*. [Available online at https://www.ncdc.noaa.gov/IPS/sd/sd.html]

NWS Springfield, cited 2016: 2013 Hollings Scholar summer project. [Available online at http://www.weather.gov/sgf/Hollings2013_MWS.]

Orlanski, I., 1975: A rational subdivision of scales for atmospheric processes. *Bull. Amer. Meteor. Soc.*, **56**, 527–530.

Pfost, R. L., and A. E. Gerard, 1997: "Bookend vortex" induced tornadoes along the Natchez Trace. *Wea. Forecasting*, **12**, 572–580.

Przybylinski, R. W., 1995: The bow echo: Observations, numerical simulations, and severe weather detection methods. *Wea. Forecasting*, **10**, 203–218.

ROC, 2012: Description document: Supplemental Adaptive Intra-Volume Low-Level Scan (SAILS). NWS/Radar Operations Center, 5 pp. [Available online at http://www.roc.noaa.gov/wsr88d/PublicDocs/ NewTechnology/Supplemental_Adaptive_Int ra_Volume_Low_Level_Scan_Description_D ocument_Final.pdf.]

Ryzhkov, A. V., T. J. Schuur, D. W. Burgess, D. S. Zrnic, 2005: Polarimetric tornado detection. *J. Appl. Meteor.*, **44**, 557–570.

Schaumann, J. S., and R. W. Przybylinski, 2012: Operational application of 0–3-km bulk shear vectors in assessing quasi linear convective system mesovortex and tornado potential. Preprints, *26th Conf. on Severe Local Storms*, Nashville, TN, Amer. Meteor. Soc., 142.

Schenkman, A. D., and M. Xue, 2016: Bow-echo mesovortices: A review. *Atmos. Res.,* **170**, 1–13.

Schultz, C. J., and coauthors, 2012: Dual-polarization tornadic debris signatures. Part I: Examples and utility in an operational setting. *Electronic J. Oper. Meteor.*, **13**, 120−137.

Skow, K. D., and C. Cogil, 2017: A high-resolution aerial survey and radar analysis of quasi-linear convective system surface vortex damage paths from 31 August 2014. *Wea. Forecasting*, **32**, 441–467.

Smith, B. T., R. L. Thompson, J. S. Grams, and C. Broyles, 2012: Convective modes for significant severe thunderstorms in the contiguous United States. Part I: Storm classification and climatology. *Wea. Forecasting*, **27**, 1114–1135.

Smull, B. F., and R. A. Houze, 1987: Rear inflow in squall lines with trailing stratiform precipitation. *Mon. Wea. Rev.*, **115**, 2869–2889.

SPC, cited 2016: Archive national sector (S4) SPC hourly mesoscale analysis. [Available online at http://www.spc.noaa.gov/exper/ma_archive/].

Stanford, M. W., J. S. Schaumann, and J. P. Gagan, 2014: A three-ingredients approach to anticipating mesovortex genesis. *13th Ann. Student Conf.*, Atlanta, GA, Amer. Meteor. Soc., S124.

Steiger, S. M., and Coauthors, 2013: Circulations, bounded weak echo regions, and horizontal vortices observed within long-lake-axis-parallel–lake-effect storms by the Doppler on Wheels. *Mon. Wea. Review*, **141**, 2821–2840.

Trapp, R. J., E. D. Mitchell, G. A. Tipton, D. W. Effertz, A. I. Watson, D. L. Andra, and M. A. Magsig, 1999: Descending and nondescending tornadic vortex signatures detected by WSR-88Ds. *Wea. Forecasting*, **14**, 625–639.

——, S. A. Tessendorf, E. S. Godfrey, and H. E. Brooks, 2005: Tornadoes from squall lines and bow echoes. Part I: Climatological distribution. *Wea. Forecasting*, **20**, 23–34.

——, and M. L. Weisman, 2003: Low-level mesovortices within squall lines and bow echoes. Part II: Their genesis and implications. *Mon. Wea. Rev.*, **131**, 2804–2823.

Van Den Broeke, M. S., 2015: Polarimetric tornado debris signature variability and debris fallout signatures. *J. Appl. Meteor. Climotol.* **54**, 2389–2405.

Wakimoto, R. M., 1983: The West Bend, Wisconsin storm of 4 April 1981: A problem in operational meteorology. *J. Clim. Appl. Meteor.*, **22**, 181–189.

——, H. V. Murphey, A. Nester, D. P. Jorgensen, and N. T. Atkins, 2006a: High winds generated by bow echoes. Part I: Overview of the Omaha bow echo 5 July 2003 storm during BAMEX. *Mon. Wea. Rev.*, **134**, 2793–2812.

——, ——, C. A. Davis, and N. T. Atkins, 2006b: High winds generated by bow echoes. Part II: The relationship between the mesovortices and damaging straight-line winds. *Mon. Wea. Rev.*, **134**, 2813–2829.

Weisman, M. L., 1992: Convectively generated rear-inflow jets in the evolution of long-lived mesoconvective systems. *J. Atmos. Sci.*, **49**, 1826–1847.

——, 1993: The genesis of severe, long-lived bow echoes. *J. Atmos. Sci.*, **50**, 645–670.

——, and R. J. Trapp, 2003: Low-level mesovortices within squall lines and bow echoes, part I: Overview and dependence on environmental shear. *Mon. Wea. Rev.*, **131**, 2779–2803.

Wheatley, D. M., and R. J. Trapp, 2008: The effect of mesoscale heterogeneity on the genesis and structure of mesovortices within quasi-linear convective systems. *Mon. Wea. Rev.*, **136**, 4220–4241.

——, ——, and N. T. Atkins, 2006: Radar and damage analysis of severe bow echoes observed during BAMEX. *Mon. Wea. Rev.*, **134**, 791–806.

Wilczak, J. M., D. E. Wolfe, R. J. Zamora, B. Stankov, and T. W. Christian, 1992: Observations of a Colorado tornado. Part I:

Mesoscale environment and tornadogenesis. *Mon. Wea. Review*, **120**, 497–521.

WMO AMDAR Panel, 2007: The international AMDAR program. World Meteorological Organization Information Flyer, 12 pp. [Available online at https://www.wmo.int/pages/prog/www/GOS/ABO/AMDAR/publications/Final%20Production%20AMDAR%20Flyer.pdf.]

WSEC, 2006: A recommendation for an enhanced Fujita scale (EF-scale). Wind Science and Engineering Center Rep., Texas Tech University, 108 pp. [Available online at http://www.depts.ttu.edu/nwi/Pubs/FScale/EFScale.pdf.]

Wurman, J., and K. Kosiba, 2013: Finescale radar observations of tornado and mesocyclone structures. *Wea. Forecasting*, **28**, 1157–1174.

REVIEWER COMMENTS

[Authors' responses in *blue italics*.]

REVIEWER A (Michael C. Coniglio):

Initial Review:

Recommendation: Accept with major revisions.

General Comments: This paper presents an analysis of a double-QLCS event characterized by multiple mesovortices and confirmed tornadoes. This case is worthy of a formal publication because 1) it is scientifically interesting and noteworthy, and 2) the presence of MVs near a terminal Doppler weather radar and the availability of SAILS scans. It is well-written and organized, and the well-sourced background material motivates the need for documenting complex QLCS events like the 30 June – July 1 event. Interpretations and conclusions made from the analyses are sound and do not overly stray into speculation for the most part.

A main concern deals with the quality of the figures. Some of this discomfort with the analysis (described in detail below) may just be related to the limitations of describing rapidly evolving convective processes with static images, but there are several instances where I think the authors argument can be clarified with better figures. I'm not sure how EJSSM handles this, but supplemental material in the form of animations could be provided that show the processes described in the paper. *[Editor's Note: EJSSM not only accommodates animations and multimedia files, but encourages and welcomes them. Several EJSSM manuscripts hyperlink from static representative figures in the published PDF to animations that, upon publication, are stored on the EJSSM server for link permanency. The authors strongly should consider this idea in light of the reviewer's comments.]*

I'm also concerned about the authors' identification of MVs (described some below) and animations of the event could help to clear up these concerns.

While the edits I recommend are mostly minor in nature, they could amount to a fair amount of work, thus I am recommending major revisions are needed before the manuscript can be considered for publication in EJSSM.

We thank the reviewer for his thoughtful and careful review of the manuscript and hope that his concerns are alleviated in the revised manuscript and the responses below.

Specific (major) comments: The word derecho is used in the title and elsewhere, but the authors never present evidence that the swath of wind reports meet the established criteria for a severe wind event to be called a derecho. I'm not one that thinks the criteria set forth in Johns and Hirt (1987) and recently updated in Corfidi et al. (2016) needs to be followed strictly, but some evidence that these were in fact something close to what can be called a derecho needs to be presented.

This was resolved with specifics in the density of severe-wind reports and the length and width characteristics of all the reports associated with each derecho, showing they qualify for both the traditional 1987 and proposed 2016 definitions.

A summary figure of all of the MVs listed in Table 1 would be informative for the reader to assess the scope of the event.

Figure 1 of this draft serves as an overview of MV and tornado tracks from the second derecho.

I encourage the authors to show analyses of the aircraft soundings and VAD wind profiles since these data are often not provided in these types of case studies when they should be used more often.

We have added an AMDAR sounding as Fig. 5 in the revised manuscript to illustrate the extreme SRH of the environment ahead of the second QLCS.

Based on the figures and what the authors are calling an MV, I wonder if these criteria for identifying an MV are too lenient. For example, what if 15 m s^{-1} was used instead of 10 m s^{-1} in criterion #1?

Furthermore, criterion #2 seems pretty vague ("perhaps not meeting previously-proposed thresholds"). It sounds like the authors are being highly subjective (hand-wavy) here. Please describe how this criterion was applied.

All but two vortices met the 10 m s^{-1} criteria. Both of those vortices (G-3 and AL) were >70 km away from the nearest radar. G-3 was a transient vortex that appeared in both KLOT and KIWX data as the broader mesovortex "G" was dissipating, and AL, although only having a peak V_{ROT} of just over 8 m s^{-1}, had a persistent TDS and reports of damage that were never officially surveyed. Each of these features still had a peak V_{ROT} rounding to 8 m s^{-1}. We have modified the discussion about the criteria in general to specify that identifiable rotation was evident in each mesovortex and that the other three criteria were used to build confidence. We are hesitant to raise the criteria beyond that because of the previously aforementioned case of mesovortex AL and because several mesovortices contained well-defined TDSs but maximum V_{ROT} values between 10 and 15 m s^{-1}. Furthermore, we have clarified the TDS criteria as follows: "A TDS or similar depression in cross-polar correlation coefficient (ρ_{hv}), owing likely to debris, that in most cases met the criteria defined by Clayton et al. (2016) and Skow and Cogil (2017)." Further comments on TDS identification can be found [under the next comment below].

The feature pointed out as a TDS in correlation coefficient doesn't appear to be a TDS to me since Z is very low there (upper-most left panel in Fig. 5). Did the authors make sure there was sufficient Z for the identified TDSs? This makes me question how accurately the authors applied criterion #2.

We utilized the 30 dBZ threshold from Schultz et al. (2012). And per recent work by Skow and Cogil (2017), we are less focused on strict correlation coefficient criteria so long as Z is outside the range of large rain drops. This is particularly the case for 30 June–1 July, where work by Clayton et al. (2016) showed that the likelihood of hail in the lowest tilts of radar data was fairly low, particularly for signatures close to the scanning radar, given a wet bulb zero level of ≈4.7 km AGL.

Figure 6: It seems odd that MVs would have made a discontinuous jump to the northeast like what is shown here for B and C. If there are no other times with data to make this determination other than what's shown on Fig. 7, I don't see how the authors can be confident that the areas of rotation shown at 0239 UTC for B and C are indeed continuations of B and C and not some other feature. For the case of B, there's quite a bit of ambiguity to where the center of B is at 0239 UTC based on Fig. 7. It's questionable whether an MV still exists or if it has been sheared out by this point. Perhaps animations would help here.

An animation of the evolution of MVs B, C, D, and the start of G has been added as Fig. 10.

Figure 9: Is there really an MV yet at 0309 and 0316 UTC? This looks more like horizontal shear vorticity induced by a rear-inflow surge nearing the ground at this point.

The loop in Fig. 12 has been created to show the evolution of the large mesovortex from when it forms near Morris, IL, to when it splits into two MVs east of Manteno, IL.

[Minor comments omitted…]

Second Review:

Recommendation: Accept with minor revisions.

Recommendation: Accept pending minor revisions

General Comments: I appreciate the authors' consideration of my previous comments. I'm satisfied with many of them. The addition of the animations vastly improves the ability of the reader to follow the discussion of the evolution of the mesovortices. However, I still am not sure there's enough evidence presented to support the authors' characterization of how some of the MVs evolved (specified below). But as I see it, a precise deterministic description of how the MVs evolved isn't necessary to meet the goals of the paper, which are to document the complexity and sheer number of MVs in this case, as well as to hypothesize on the generation mechanisms.

    In other words, I think the authors could allow for more uncertainty in how the MVs are defined and evolved (after all it's hard to say with much certainty what's happening from single Doppler, even if it's high temporal resolution), while still maintaining a strong documentation of this scientifically interesting event. This would require some rewriting and reconfiguring of some of the figures showing the MV tracks, but I think this would fall under minor revisions.

We thank the reviewer for his thoughtful insights into the analysis. We hope that our explanations below alleviate any outstanding concerns.

Specific concerns on MV characterization:

The animation shown in Fig. 11 is very helpful, but I still don't see enough evidence to support the hard left turn between 0236 and 0239 UTC for both MVs. It looks possible that B simply decays and C moves to the location of where you have B at 0239 UTC, with D being a separate strong MV.

The above interpretation was considered in the analysis, but ultimately the analysis stated in the paper was favored for three reasons. The first is that two maxima in inbound and outbound Doppler velocity are present at 0239 UTC, the time at which "C" is roughly estimated to have merged with "D". The second reason was that a marked increase in the intensity of "D" and an EF1 tornado event occurred around the time of this merger, consistent with behaviors shown in Weisman and Trapp (2003). The third reason is that the turn of MV "B" to the left (toward the east) appears to be more gradual and resolved within the 0.5° SAILS scans from KLOT. In fact, there is some indication that "B" may have still been a separate entity just east-southeast of "D" at 0241 UTC, but we did not feel confident enough of that in our analysis to catalog "B" at that time as that would be a bit too speculative. We certainly cannot completely rule out the evolution given by the reviewer, but feel that the interpretation in the paper fits more closely with the observed behavior of the mesovortices.

Fig. 13: I'm still unsure that G split into two subvortices as described. This would be a very unique (and strange) dynamical event that would require more explanation. It's hard to determine this evolution with as much certainty as conveyed by the authors with single Doppler, even if it's high temporal resolution. For example, the MV over Wilmington at 0303 UTC doesn't look like a continuation of the MV that was south of Minooka several minutes prior, but rather a separate spin up. And I'm not sure there's really an identifiable MV ~0308–0318 UTC, but rather a broad rear-inflow push prior to the development of G-1 and G-2. I suggest the authors back off on their characterization of a splitting MV.

Our interpretation is that "G" remains present from its 0248 UTC genesis to the split. This interpretation was made by noting that the maximum outbound Doppler velocity values in the rear-inflow region were matched with a region of enhanced inbound velocities to the east, leading to a broad region of cyclonic to cyclonic-convergent flow. It should be noted that the "split" that we identified occurred right as this portion of the line interacted with the remnant thermal boundary from the first QLCS. Eventually, the boundary drifted north to intersect "G-1", which we believe it why it was stronger, larger, deeper, and more tornadic. We certainly agree that this "split" is both unique and strange, and it certainly does call for more explanation and investigation. However, such investigation, including numerical simulation,

seems simply beyond the scope of this paper, given the already substantial amount of information presented.

Fig. 19: I found the storm-relative animation more difficult to follow than the other ground-relative animations, but maybe that's just personal preference (or maybe it's because the data is every 5 minutes here). Regardless, I'm not sure there's enough there to say V is a distinct MV. It almost looks like a weak downdraft from the cell that gets ingested into the oncoming convective line.

Due to the already-substantial number of and detail within the figures of this paper, we opted to only show the 0.5° elevation scan evolution of this sequence. However, in our interpretation, "V" lasted three volume scans with vertical continuity of rotation through several tilts. There was no indication of divergence in the signature, let alone a dominance in divergence that would likely be expected with a downdraft signature at the lower elevation tilts of a nearby downburst. "V" was also not the only MV to form in the convection ahead of the original QLCS. "AE" showed a similar behavior as discussed in Section 4b.2. For this reason, we remain compelled to leave the identification of MV "V" as-is, owing to a preponderance of the evidence leaning toward it being a vortex.

[Editor's Note: At the Editor's request, the authors added a paragraph at the beginning of section 4 to state the existence of uncertainty regarding several of the mesovortex morphologies, such as those discussed above, while still representing their analyses as most-probable scenarios.]

 [Minor comments omitted…]

REVIEWER B (Adam J. French):

Initial Review:

Recommendation: Accept with major revisions.

General comments: This is an interesting study that documents a number of unique and complex mesovortex behaviors and interactions within the second of two damaging MCSs to affect the IL-IN-OH region 30 June–1 July 2014. The authors do a nice job of analyzing the mesovortices using available WSR-88D data including polarimetric fields and high-temporal frequency base scan data from the SAILS/MESO-SAILS scan strategies. I do have some suggestions for some additional work to clarify a few points, as well as a few concerns, as outlined in the comments below. I think this work will be a useful addition to the severe-storms literature base, provided that these comments are addressed. Since addressing the comments will require some additional analysis, I am recommending major revisions.

We thank the reviewer for his careful and detailed review and hope that his concerns are alleviated with the revised manuscript and responses below.

Substantive comments: I would like to see some more discussion of the overall event before diving into the specific "special case" mesovortices. While clearly the focus of the paper was on some of the unique mesovortex behavior observed, having a little more storm-scale to mesoscale context would be helpful in interpreting the results and understanding the importance/relevance of the observed behaviors. Specifically, I think the addition of a figure, and some brief discussion of a WSR-88D scale radar overview of MCS #2 would be helpful in bridging the regional scale overview shown in Fig. 1 and the mesovortex-scale, detailed analysis shown in subsequent radar images (e.g., Figs. 4, 5,7, etc.).   This would be helpful to gain some context into how the overall system was evolving as the different mesovortex features were ongoing. Another idea would be to add an overview mesovortex track plot illustrating the full set of mesovortices shown in Table 1. Perhaps this would be too much for one figure, but as I looked some of the other mesovortex track figures (e.g. Figs. 4a, 6, 11, 14, 16) I kept wondering how these tracks fit in the "big picture" and if they would stand out as being unique compared to the rest of the tracks. Given the large number of vortices produced (39 listed in Table 1) I think it can be easy to lose the forest

for the trees in a sense by focusing on the special cases. *[Editor's Note: The comments of Reviewer A regarding animations are relevant here too; some form of animated sequence(s) would help reviewers and readers to visualize the continuity of these features better as well.]*

We have added an overview map (Fig. 1) to frame the entire event relative to the discussions of some of the individual mesovortices.

In a similar vein to the previous comment, I would like to see a little more analysis of the mesoscale environment in the wake of MCS 1. Figures 2 and 3 do a nice job of summarizing the regional scale features, but it would seem like a more focused analysis of the post- MCS 1 environment would be relevant here as well. Was there evidence of any outflow boundaries, local convergence lines, or other features that could have influenced mesovortex behavior? I think this would be of particular interest in analyzing some of the longer-lived or stronger vortices (e.g. G, K, etc.). Furthermore, the apparent "corridor" of mesovortex activity shown in Fig. 11 (mesovortex G and those that developed downstream after it dissipated) would suggest there may be some external element favoring mesovortex production with this portion of the MCS. Did any of these appear to form or track along any features left in the wake of MCS 1? Since the surface map provided in Fig. 2 is at 00 UTC, prior to MCS 1 crossing Indiana, the reader cannot really evaluate this.

A more thorough description of the mesoscale environment in the wake of the first derecho has now been provided in the paper.   In addition, a figure was added to highlight the surface conditions at a time between the two derechos that depicts the northward moving outflow boundary that would serve as a key focus for mesovortexgenesis.

I found section 4b3, the discussion of the smaller mesovortices following mesovortex G to be a little overly speculative at points, namely in terms of suggesting the presence of possible tornadoes associated with several mesovortices based on inferred TDS signatures alone. In particular, in looking at figure 13 there appears to be a rather widespread region of depressed associated with the cluster of mesovortices. Could this perhaps due to debris being lofted by straight-line winds associated with the mesovortices? I am not aware of any past research that has looked at debris signatures with "straight-line" winds, but it would not seem out of the question that this is possible. Did any of the confirmed tornadoes produce TDSs? My understanding is that a TDS usually implies a somewhat strong tornado, so if these were all relatively weak it would seem unlikely that they would be producing substantial TDS (although I suppose this might depend on what was being damaged).

Another reason that I am a bit skeptical of the TDS-inferred tornadoes is that the statistics on the "possible tornado" cases (Figures 18–23) all seem to indicate "weaker" mesovortices (smaller, depth, diameter), which to me seems surprising.   To be clear, I am not discounting the idea that there may have been weak tornadoes with these vortices, but I just do not feel that the evidence presented supports this strongly enough. Perhaps an alternative would be to include other possible explanations for the depressed in addition to the possibility of them being due to a TDS.

We acknowledge the reviewer's hesitancy toward the identification of several of the features that have been labeled TDSs as TDSs. We refer to these features as TDSs for the following reasons.

(1) As per Schultz et al. (2012), TDSs can be detected in tornadoes as weak as EF0.

(2) Although no tornadoes were confirmed with R, T, or Z, R and Z were not surveyed, and T was only surveyed at one location.

(3) The debris signatures reached as high as ~1370 m AGL. Though we are aware of findings from Mahale et al. (2012, Wea. Forecasting) of debris associated with nontornadic winds, we are dubious of nontornadic winds being able to loft debris to that height.

(4) The large cluster of depressed correlation coefficient is likely best explained by the fallout of debris from each individual circulation (see Van Den Broeke 2015). To assume that it were caused by straight-

line winds when these vortices were present would likely be over-speculative given the known and documented occurrence of debris fallout being sampled by polarimetric radar.

[Editor's Note: Though originally termed "minor", the comments below appeared scientifically substantive enough to merit inclusion here.]

Details of mesovortex identification criteria: I question whether criteria 2 and 3 are really sufficient to identify a mesovortex. For criteria 2, I think the presence of a depression in is a good additional data point in identifying a mesovortex, but should only be used in addition to the appearance of a rotational signature in the velocity data. Were there any vortices that were identified solely on the basis of? Similarly with number 3, while most QLCS tornadoes are found to be associated with mesovortices, I do not know that it is a necessary condition. I could see either of these being used as additional evidence of the presence of a mesovortex, but this should be in addition to a velocity signature. Since the wording states "at least one of the following four criteria was met" to me this suggests that either one of these could be used by themselves to identify a mesovortex. If, instead these are just used to make the case for circulations that do not meet the threshold value in criteria 1 I think that would be reasonable, but needs to be clarified.

All but two vortices met the 10 m s^{-1} V_{ROT} criteria. Both of those vortices (G-3 and AL) were >70 km away from the nearest radar. G-3 was a transient vortex that appeared in both KLOT and KIWX data as the broader mesovortex "G" was dissipating, and AL, although only having a peak V_{ROT} of just over 8 m/s, had a persistent TDS and reports of damage that were never officially surveyed. Each of these features still had a peak V_{ROT} rounding to 8 m s^{-1}. We have modified the discussion about the criteria in general to specify that identifiable rotation was evident in each mesovortex and that the other three criteria were used to build confidence. Furthermore, we have clarified the TDS criteria as follows: "A TDS or similar depression in cross-polar correlation coefficient (ρ_{hv}), owing likely to debris, that in most cases met the criteria defined by Clayton et al. (2016) and Skow and Cogil (2017)."

Discussion of MV "E" and "F": Was there any relation between the apparent Fujiwhara effect between these two vortices and the wind damage/tornado produced? In other words, aside from being an interesting behavior, did this appear to have an effect on mesovortex evolution such that it impacted severe weather production?

We suspect an additional tornado formed immediately after the merger of "E" and "F". However, the ground clutter around KLOT and the lack of an official survey conclusion of "tornado" led us to not mention this in the paper so as to avoid excessive speculation. These observations, however, did lead us to identifying "E" as a "possibly tornadic" mesovortex.

Since both mesovortices AB and AC are evident in the Doppler velocity data, I suspect there would be at least some indication of one vortex rotating around another in these data. Rather, could the path of the tornado also be explained simply by a tornadic circulation smaller in scale than the mesovortex rotating around vortex AC? Does the width of the tornado track imply that this was unlikely (i.e., the damage path being similar in scale to the mesovortex)?

The tornado track was only 970 m long by 140 m wide. Because MV "AB" (note the nomenclature change due to combining the original "T" and "AA") averaged over 2.8 km in diameter, we have added to the discussion the alternate possibility that the tornado was rotating within the larger MV "AB".

Does the development of the new line ahead of the original line appear to be related to discrete propagation (e.g., Fovell et al 2006, *Monthly Weather Review*)? Is there any indication of a bore or other feature emanating from the original line that may have triggered the second line? Given the time of day it would stand to reason that the system could be becoming elevated, or perhaps interacting with outflow from the previous MCS in such a way as to trigger a bore.

We believe that a bore and potential additional solitary waves ahead of it (e.g. Knupp 2006) likely played a critical role in the entire evolution of the 2nd QLCS. This analysis is still ongoing and we plan to submit an

entire separate paper on the subject if/when we feel comfortable enough with the amount of supporting evidence and analysis we have.

It is striking to me that there appears to be a "corridor" of enhanced mesovortex activity associated with this portion of the line. That it at least briefly continues ones the new line forms further east suggests to me that perhaps there is something like an external boundary having an influence. Is there any evidence of this? (see substantive comment #2 above).

Many of the mesovortices and tornadoes indeed occurred on a left-over thermal boundary from the first QLCS. See the new Fig. 6 and associated text for more details.

[Minor comments omitted…]

Second Review:

Recommendation: Accept with minor revision.

General comments: The authors have done a nice job of addressing my comments on the first draft. I particularly like the new figures 1 and 6, which help to provide a nice overview of the event. Also, the addition of animations to a number of the radar figures really helps to illustrate the vortex behaviors of interest. One additional comment I have regarding the content has to do with the trochoidal oscillation observed with vortex G2 (page 13 bottom of the right-hand column). In reviewing the updated figures, as well as looking at the 88D data some myself, I am having a hard time seeing this oscillation. I suggest removing this discussion since 1) its presence seems to be somewhat in the eye of the beholder, and 2) it does not appear to be a central part of the storm's evolution (i.e., connected to a substantial change in vortex intensity, severe weather production, etc.). Other than this, and the minor editorial comment noted below, I think the revised manuscript is acceptable for publication.

We thank you for the thoughtful comments and suggestions you have provided during the review process. We have removed the trochoidal oscillation discussion and the corresponding Kuo (1969) citation.

[Minor comment omitted…]